Addis Ababa University

SCHOOL OF GRADUATUE STUDIES

DEPARTMENT OF PHYSICS

The effect of El Niño-Southern oscillation (ENSO) on the Ethiopian Rainfall Pattern

Robel Getachew Worku

A THESIS SUBMITTED TO THE DEPARTMENT OF PHYSICS PRESENTED IN PARTIALFULFILLMENT OF THE REQUIREMENTS FOR THE DEGREE OF

MASTER OF SCIENCE (PHYSICS)

ADDIS ABABA UNIVERSITY

ADDIS ABABA, ETHIOPIA

JUNE 2012

ADDIS ABEBA UNIVERSITY

DEPARTMENT

OF

PHYSICS

Approval of the Board of Examiners

Supervisor: _____

Dr. Elias Lewi

Examiners: 1. Dr. Gizaw Mengistu

Signature: _____

2. Dr. Lemi Demeyu

Signature:_____

Acknowledgements

First and for most, my greatest thanks goes to my advisor Dr. Elias Lewi and for his close guidance, valuable criticism, advices, and support in completion of this thesis and writing the report.

I am greatly indebted to my whole family for their help, care and support throughout my thesis work from beginning up to end with financial and courage moral support.

I would like to extend my thanks to National Meteorological Service Agency (NMSA) of Ethiopia, the National Climate Data Center (NCDC) and Climate Prediction Center (CPC) for the metrological data that has been used in this thesis free of charge.

I am also thankful to all my friends and classmates for their constant encouragement and cooperation.

Finally, I would like to express my gratitude to all people that have spent their precious time to bring this work to a success.

Table of Contents

List of tables

List of Figures

Acronyms

CMAP = Climate prediction center Merged Analysis Precipitation

CPC = Climate Prediction Center

ENSO = El Niño-Southern Oscillation

FAO = Food and Agricultural Organization

FFT = Fast Fourier Transform

IFFT = Inverse Fast Fourier Transform

IPCC = Intergovernmental Panel for Climate Change

IRI = International Research Institute

ITCZ = Inter Tropical Convergence Zone

NMSA = National Meteorological Service Agency

NOAA = National Oceanic and Atmospheric Agency

ONI = Oceanic Nino Index

RF = Rain Fall

RFA = Rain Fall Anomaly

SLP = See Level Pressure

SO = Southern Oscillation

SOI = Southern Oscillation Index

SST = See Surface Temperature

SSTA = See Surface Temperature Anomaly

Abstract

This study is focused on the first step to investigate the interdependence between El Niño-Southern Oscillation (ENSO) and the rainfall pattern in the Ethiopian diverse micro-climate zones, using correlation and spectrum analysis. For this purpose, the sea surface temperature in the pacific and the measured rainfall in the diverse micro-climate zones have been used as parameters. The investigation was made by filtering the desired data and then directly correlating long period data both in time and frequency domain. The correlation analysis in the time domain on one hand showed that the rainfall in most locations in the north western, north east and central part of Ethiopia have a strong negative correlation with ENSO. The average time lag for these negatively correlated values is found to be 4 to 12 months after the occurrence of ENSO. On the other hand some few locations in the south and south eastern parts of Ethiopia showed very weak positive correlation. The result from the spectrum analysis also showed that the periods nearly 3 to 5 years play a crucial role in the pattern of the rainfall in Ethiopia. The cross-spectrum analysis in general showed that the 3.5 to 5 years periods play crucial role in the influence of ENSO. The result can also be used to forecast the relative intensity of rainfall on the basis of the occurrence of ENSO.

Unit 1

Introduction

1.1 Background

The impact of climate change is expected to be the most severe on developing countries especially on the ultra-poor, partially due to low economic performance. Many low income countries are located in tropical, sub-tropical region, or in semi desert zones, which are particularly vulnerable to shifting weather patterns and rising temperature (Joachin, 2008). Regional patterns of poverty and hunger within countries also show that the world‘s poorest are often located in geographically adverse zones. For example the most food insecure regions in Ethiopia are those that experience both the lowest and the most variable rates of rainfall (RF).

The Intergovernmental Panel for Climate Change (IPCC, 2001) has stated that as a result of climate change least developed countries including Ethiopia will experience a range of adverse impacts. Diminished resource exacerbates due to desertification, increased transmission of vector disease, and there are also predictions of increased incidence extreme event and gradual change that could jeopardize national efforts in poverty reduction economic growth and sustainable development. Climate change could affect poverty reduction strategies of developing countries. Of all the regions affected by climate change, Ethiopia, is characterized by diverse micro climates (NMSA, 1989) and is very sensitive to climatic changes in particular to rainfall variation.

Variability of rainfall is believed to be variations of tropical oceanic and atmosphere interaction, especially El Niño-Southern Oscillation (ENSO) (Haile, 1988). As climate change like ENSO leads to decrease in yields, in developing countries, it will further exacerbate food security (Joachin, 2008).

Ethiopia‘s climate is influenced by general atmospheric and oceanic factors that affect the weather system and the time of inception and intensity of the rains (Bekele, 1997). The summer rainfall contributes about 74% of the annual rainfall in the country. Therefore, the failure of the summer rainfall has disastrous consequences upon the country and the rest of East Africa. It has been affected by recurrent drought for a long time. The failure of seasonal rainfall adversely affects the country‘s socio-economy, in particular food production (Babu, 199b). To alleviate this problem different research work has been carried out and result indicated that the major cause of frequent drought in Ethiopia is climate variations across the country especially rainfall variation (Babu, 199b).

Rainfall in Ethiopia is largely the result of the migration of the Inter Tropical Convergence Zone (ITCZ). Findings show that ITCZ is highly sensitive to El Niño-Southern Oscillation (ENSO). The National Meteorological Service Agency (NMSA) of Ethiopia believed that, ENSO is

strongly related to rainfall distribution in the country (Babu, 1999b). Researchers at NMSA and policy makers in Ethiopia believe that the state of sea surface temperatures (SSTs) in the tropical Pacific Ocean affect Ethiopian climate through teleconnections (Haile, 1988). NMSA also believes that the Atlantic and the Indian oceans' SST anomalies (SSTA) affect Ethiopia. Other studies also support the NMSA's conclusions. For example, the variability between high and low flood levels of the Nile River, whose major water source is highlands of Ethiopia, is related to the ENSO cycle (Quinn, 1992).

Apart from repeated drought experiences in Ethiopia, there is no properly documented information on past and current climate variability and its impact on the society, the environment and the economy of the country. As a result, development projects envisaging food security, resource management and rural development failed to consider climate variability and long-term climate change (Mahdi and Sauerborn, 2002). The major problem and primary reason for this is lack of systematically documented database and information on long-term rainfall variability in the country.

1.2. Statement of the problem

The aforementioned research work were based on short periods of data, direct drawing and correlation values of the relation between rainfall and SSTA for a few locations as generalized. But Ethiopia as a diverse microclimate, the current work was focused in the study of detail mathematical and scientific facts of data analysis of ENSO with different climatic zones. For this purpose rainfall data from different weather stations in the different climatic zones of Ethiopia were used. However due to sparse distribution of stations and because of the reason that data at some station is not continuous, the Satellite estimated rainfall has been an essential supplement to the ground observation and it was important to interpolate missed rain gauge data. Direct merge of satellite data to missed rain gauge is not possible (Dinku, 2007).

Climatic conditions are periodic, even drought, floods, and climate change epidemic disease are frequently occurred. For the purpose of detail warning, we have to do detail analysis of the relation between ENSO event and RF variability for each diverse microclimate zone with a long period of time. Full considerations must be given for ENSO conditions whereas seasonal variations of the changes must be neglected. In addition to time domain, frequency domain or spectrum analysis will present frequently or periods having a sever effects between ENSO and RF.

All the above showed for a new technique that solve problems on the relation between ENSO and RF variability with possible predictions. The main work of this thesis is to emphasis in which diverse microclimate zone ENSO will affect and which frequency dominantly show a sever relation between ENSO and RF variability. It also tries to explain time lag between ENSO and RF for each locations.

1.3. Research objectives

1.3.1. Objective of the study

- The general objective of this study is to establish and quantify cross correlation and spectrum analysis between ENSO and RF pattern in Ethiopian diverse micro-climate zones; and then establish a means that can be used in predicting the effect of one on the other.

1.3.2. Specific objectives

- To design a means to interpolate missed data and filter out seasonal effects from the data so that the analysis can be done on the ENSO period.
- Document the correlations between ENSO and RF variation in the different climatic zones.
- Carry out spectrum analysis to study which period of ENSO is affecting the RF pattern in Ethiopia.
- Draw conclusions, limitations and recommendations of the thesis for future works.

1.4. Research questions

- ✓ Does ENSO affect all Ethiopian diverse microclimate zones?
- ✓ Which zone does ENSO affect?
- ✓ Which periods of ENSO affect the diverse microclimate zone?
- ✓ Do Ethiopian droughts possibly correlate with ENSO event? If possible can we predict the future event?
- ✓ What are the possible effects of ENSO can be observed?

1.5. Outline of the thesis

Unit 2 considers literature reviews of ENSO. Unit 3 discuss about the locations of the rain gauge, satellite status and area of interest, topography, climate regions and rainfall distributions. It also explains the possible atmospheric effects of rainfall variations and its consequences. Unit 4 gives detail explanations of data collection, scientific methods and data analysis of thesis work. Unit 5 gives result and discussion of the work and finally in Unit 6, the conclusion of the research outcome is given and recommendations are forward.

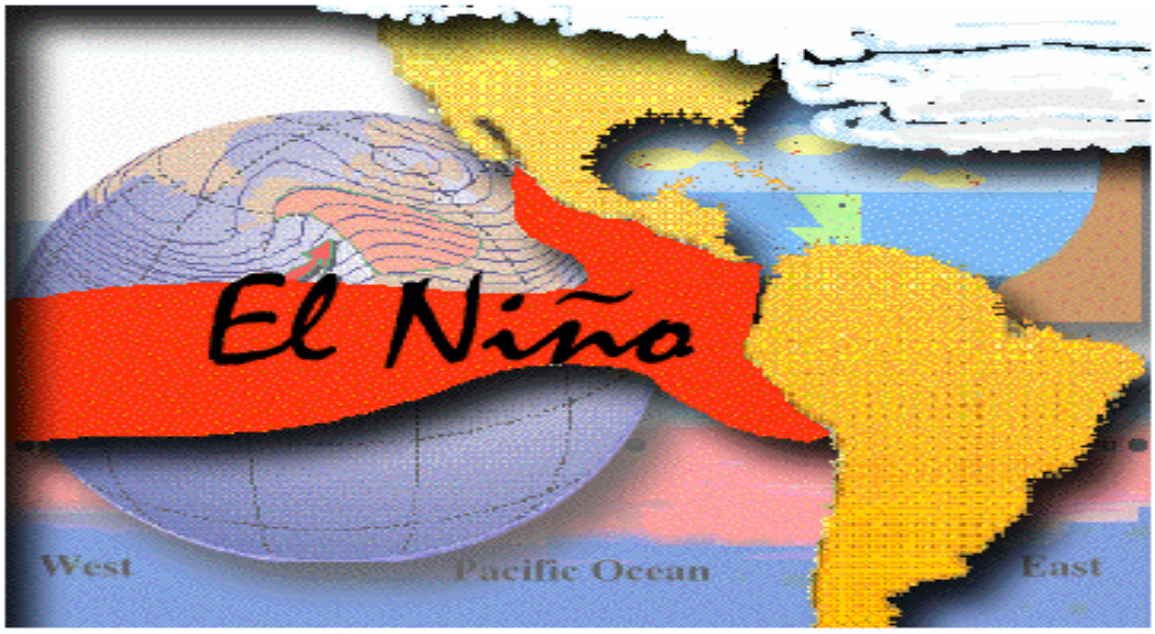

(Source: http://ww2010.atmos.uiuc.edu/(Gh)/guides/mtr/eln/home.rxml Graphics by Yiqi Shao)

Unit 2

Theory of El Niño-southern oscillation (ENSO)

- The second climate challenge in our world!

2.1 Historical Observations

Although the phenomenon is at least thousands of years old, its impacts on global climate have only recently been recognized (McPhaden et al., 1998; Neelin et al., 1998).

El Niño was observed as early as the 1600s. More systematic study began at the end of the 19th century, when Peruvian geographers noted unusual oceanic and climatic phenomena occurring periodically along the Peru coast (east of tropical pacific). They noticed that eastern Pacific warming was sometimes very strong. In the 1920s The British scientist Sir Gilbert Walker empirically identified that some notable climate anomalies–changes in atmospheric pressure and circulation–happen around the world every few years. He invented the term for those climate oscillations, ~~t~~he Southern Oscillation (SO)." While stationed in India studying the monsoon, Sir Walker observed pressure differences in the equatorial Pacific Ocean. He noticed ~~a~~ seesaw" of atmospheric pressure measured at two sites: Darwin in Australia, the Indian Ocean, and in Tahiti, an island in the South Pacific. When atmospheric pressure rises at Darwin it falls in Tahiti, and vice versa.

In the 1950s, it was observed that climate anomalies connected with the Southern Oscillation coincided in general with El Niño occurrences. Around 1960, scientists realized that the warming of the eastern Pacific is only a part of the oceanic oscillations that extend westward along the equator, out to the dateline. At about the same time the famous meteorologist Jacob Bjerknes proposed that El Niño was just the oceanic expression of a large-scale interaction between the ocean and the atmosphere, and that the climate anomalies could be understood as atmospheric "teleconnections" spreading from the warm-water regions along the equator in the mid-Pacific. Since approximately 1975 scientists have been researching El Niño and the Southern Oscillation phenomena together. Today we know that El Niño is a part of an interannual climate oscillation called the El Niño Southern Oscillation (ENSO) event. El Niño is a warm phase of ENSO, the cold phase of this event is called La Niña.

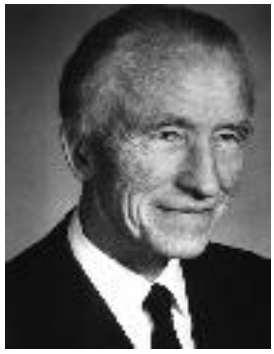

Prof. J. Bjerknes
http://www.atmos.washington.edu/gcg/RTN/rtnt.html

–El Niño" is a warm ocean current that flows along the Equator and towards the west coast of South America approximately every 3 to 7 years. It often reaches the coast in December, and is named –El Niño" after the baby Jesus whose birth is celebrated during December. (The warm ocean water pushes down cool, upwelling water, cutting off the supply of nutrients to phytoplankton (microscopic plants). With less food, many animals like fish, birds, and marine mammals die, so fishermen's incomes plummet. In addition, more rain falls, leading to floods and mudslides. At the same time that El Niño affects the east side of the Pacific, the west side of the Pacific Ocean experiences a cooling. Thus, atmospheric pressure increases in the western Pacific and decreases in the eastern Pacific. This reversal of the normal conditions in the atmosphere as mentioned above is called the –Southern Oscillation." During the last century, scientists began to recognize that El Niño, the Southern Oscillation, and other changes across the entire Pacific Ocean (the world's largest ocean) were all linked together, and came to call the phenomenon ENSO.

ENSO is the largest and best known mode of climate variability that affects weather, ecosystems and societies in large parts of the world in different phases known by El Niño and La Niña.

2.2 E l Niño phase

2.2.1 Normal Conditions

During normal conditions, the trade winds push ocean water near the Equator to the west. As the water travels near the Equator, it becomes warmer and warmer. Eventually it hits Asia, and begins to pile up, raising the sea surface on the western side of the ocean by about 3 feet (about half a meter). Gravity wants to push the water –downhill" towards the east, but the winds hold it in the west, so instead it flows –downhill" along the east coasts of Asia and Australia as western

boundary currents. The trade winds also pull water away from the west coast of South America (eastern Pacific), and water rises up from below to replace it (upwelling). Upwelling causes the thermocline (the zone at the top part of the ocean in which temperature decreases rapidly with depth) to be much shallower in the Eastern Pacific than in the western. Trade winds and the equatorial upwelling maintain warm sea surface temperatures at the western equatorial Pacific and cold surface temperatures in the east as shown in figs. 2.1-2.2.

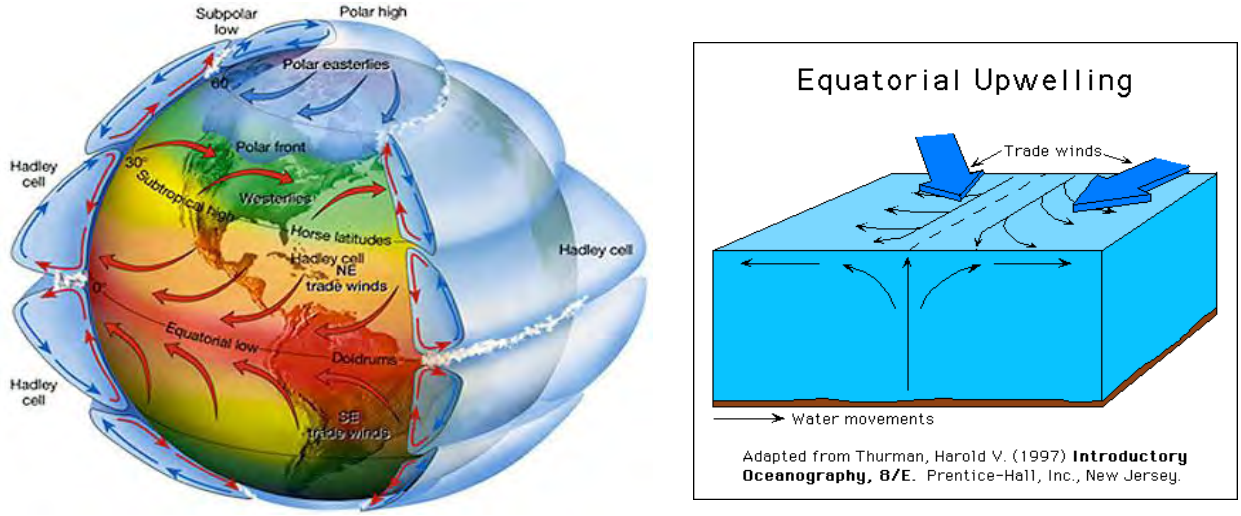

(Sources: http://iridl.ldeo.columbia.edu)

Figure 2.1: Normal distribution of atmospheric and oceanic waves across the Globe. Trade winds across the ocean surface blow from East to West along the equator and Hadley circulation along the atmosphere (left side). On the right side shows trade winds pulling oceanic water to pill up (upwelling) along the coast.

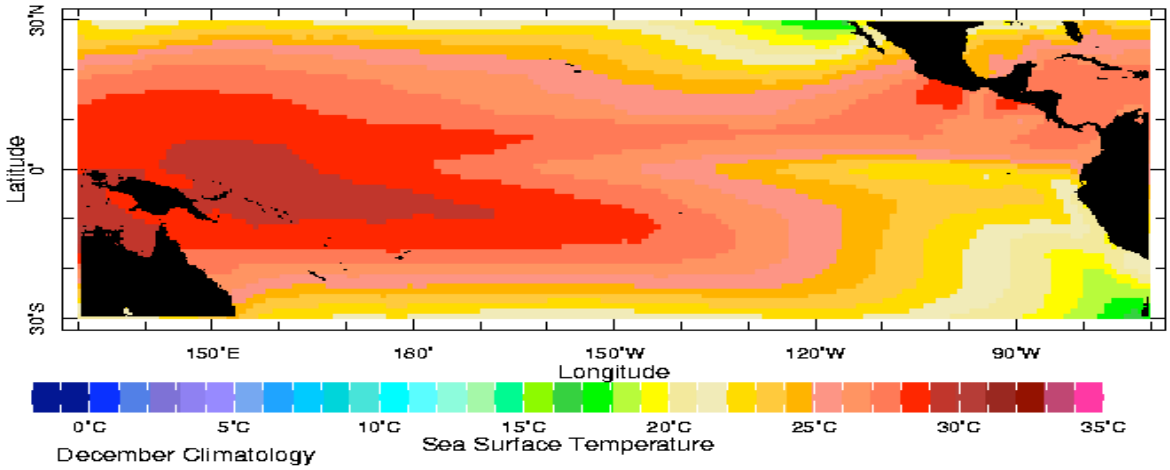

(Source: http://iridl.ldeo.columbia.edu)

Figure 2.2: Top view of equatorial pacific; as shown in this picture temperature increases west side of the pacific (deep red).

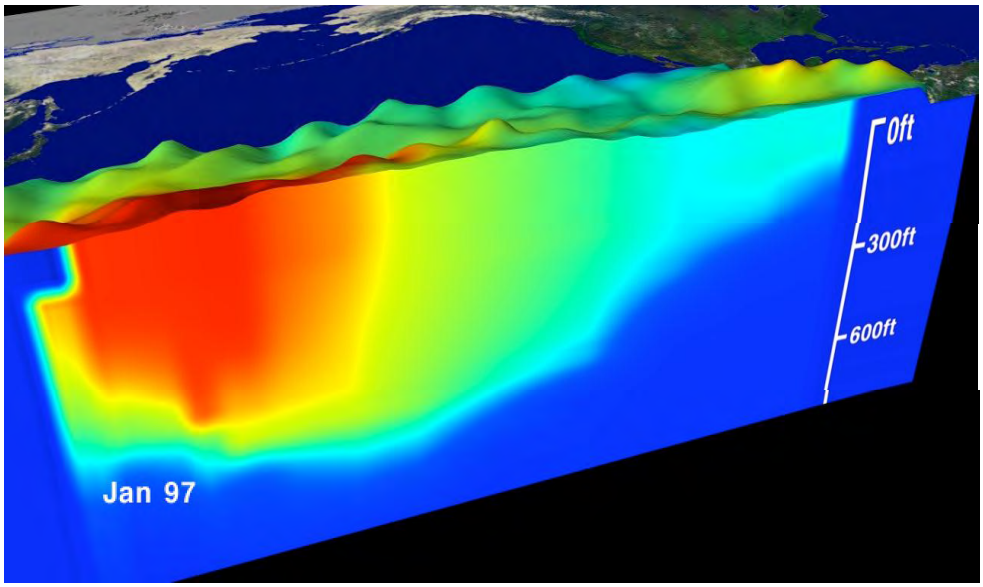

(Source: http://iridl.ldeo.columbia.edu)

Figure 2.3: Cross-sectional view of the Ocean. Pushing of ocean water by trade winds along the west side of pacific, the temperature of ocean depth vary. Along the same depth temperature becomes decrease (i.e thermocline depth decreases from west to east).

The warm water on the west side of the Pacific warms the air above it, lowering its density and causing it to rise. The air is moist owing to lots of evaporation from the warm ocean water, so as it rises and cools; the water vapor condenses, producing lots of clouds and rain. Cooler air from the east replaces the rising air, and is itself warmed, and rises. Air sinks on the cooler, east side of the Pacific, so clear skies with little rain are common there. Notice that the temperature difference between the two sides of the ocean creates winds which blow to the west. These winds cause warm water to pile up on the western side of the ocean, creating the temperature difference. Thus, the ocean water and winds reinforce one another; they are part of a ~~"p~~positive feedback loop". This positive feedback loop circulation of east-west atmospheric circulation refers to The Walker circulation (see Fig. 2.4). Its strength fluctuates with the southern oscillation.

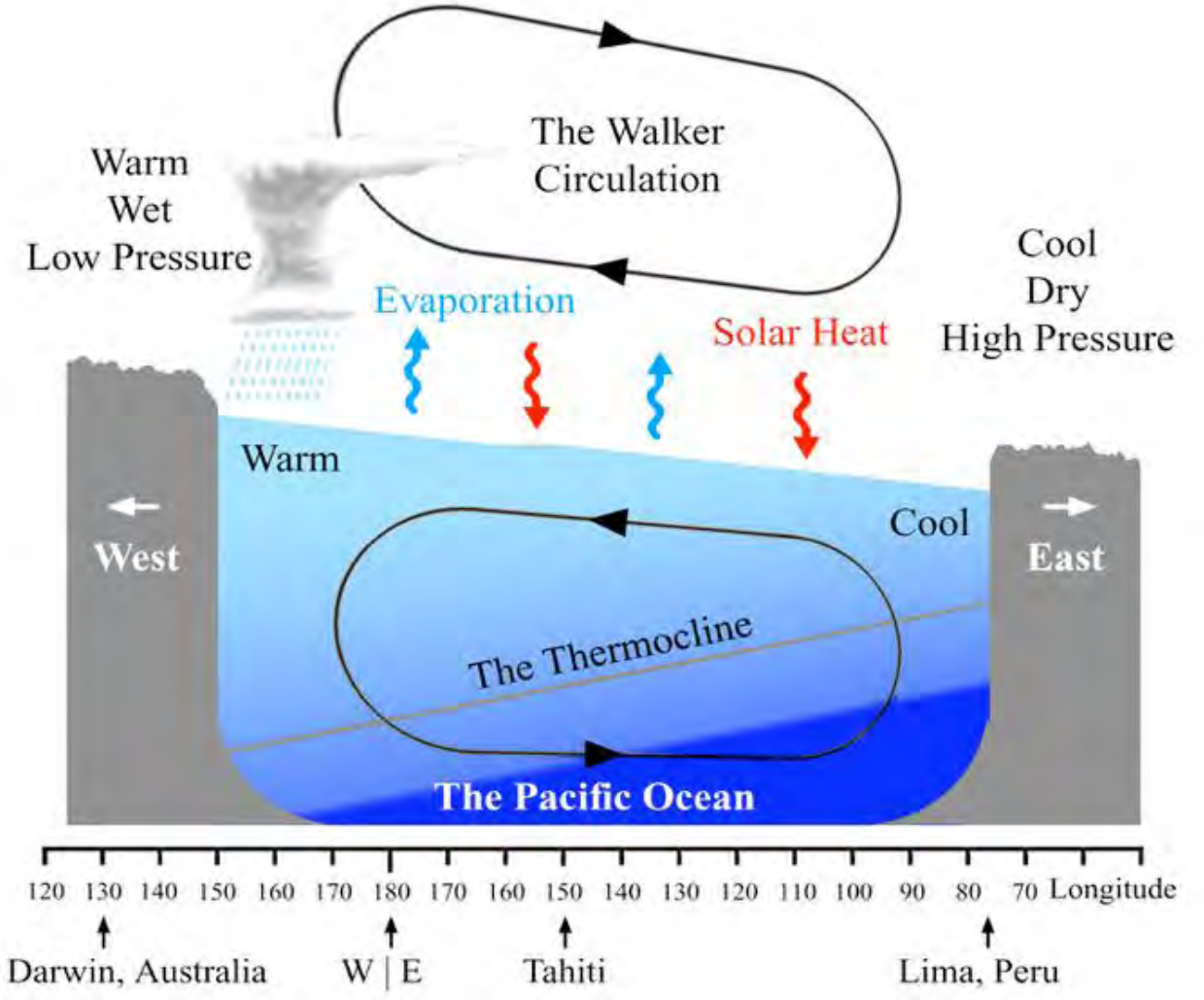

(Source: http://iridl.ldeo.columbia.edu)

Figure 2.4: A very simplified viewing of ocean-atmosphere coupling, indicates oceanic circulation inside the ocean cold water moves from deep west side to top side of east then back to west pulled by trade winds and finally moves to the deep side of warm water. In case of the atmosphere wind blows from east to west along oceanic surface and from west side to east through the atmosphere by pressure difference.

2.2.2 El Niño condition

When trade winds weaken, the equatorial upwelling decreases, the thermocline gets deeper, the ocean surface along the coast of South America becomes warmer, and trade winds weaken even

more. This in turn causes surface waters in the eastern Pacific to become even warmer and so on. This mechanism is known as the Bjerknes hypothesis and represents an onset of El Niño (Bjerknes, 1966). The questions remain: what stops warming in the eastern Pacific and why do El Niño events last approximately 12-18 months? The widely accepted (but not unique!) explanation is the delayed oscillator hypothesis. During the warming event in the eastern Pacific, the thermocline deepens along the equator and rises in the regions about 3 to 8 latitude degrees from the equator. These off-equator thermocline anomalies have little effect on the ocean surface temperature, but they propagate under the westerly ocean surface as so called Rossby waves, with a speed of about 0.8m/s.

When Rossby waves reach the Indonesian archipelago they are reflected back as another type of the ocean underwater waves, namely equatorial Kelvin waves. Because of the deep thermocline in the western Pacific, the arrival of the Rossby signal does not affect surface temperature. Kelvin waves are much faster than Rossby waves and propagate eastward along the equator with an approximately 3 m/s speed as a shallower thermocline anomaly. Each Kelvin wave takes about three months to cross the Pacific but Rossby waves traversing the Pacific in a year. When Kelvin waves reach the equatorial Eastern Pacific, they move the thermocline (and, therefore, cold water deeps) in this region. On the other hand thermocline on west side ups to the ocean surface. Closer to the surface, cool the ocean‘s surface and terminate the warm on set of El-Nino event in the west side (Glebushko, 2004). The amplitude of the Kelvin waves indicates the magnitude of changes along South American coast. In addition, the warm water of El Niño warms east side of the air and produces lots of evaporation.

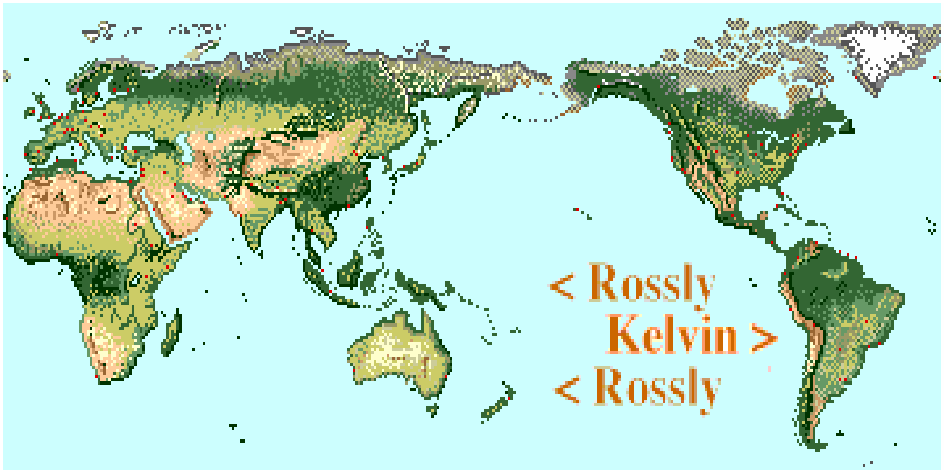

(Source: http://www.usafa.af.mil/dfp/physics/webphysics/jittworkshop/ 152Sp98GFelNino.html)

Figure 2.5: *The apparent motions of Rossby and Kelvin waves* across the tropical pacific.

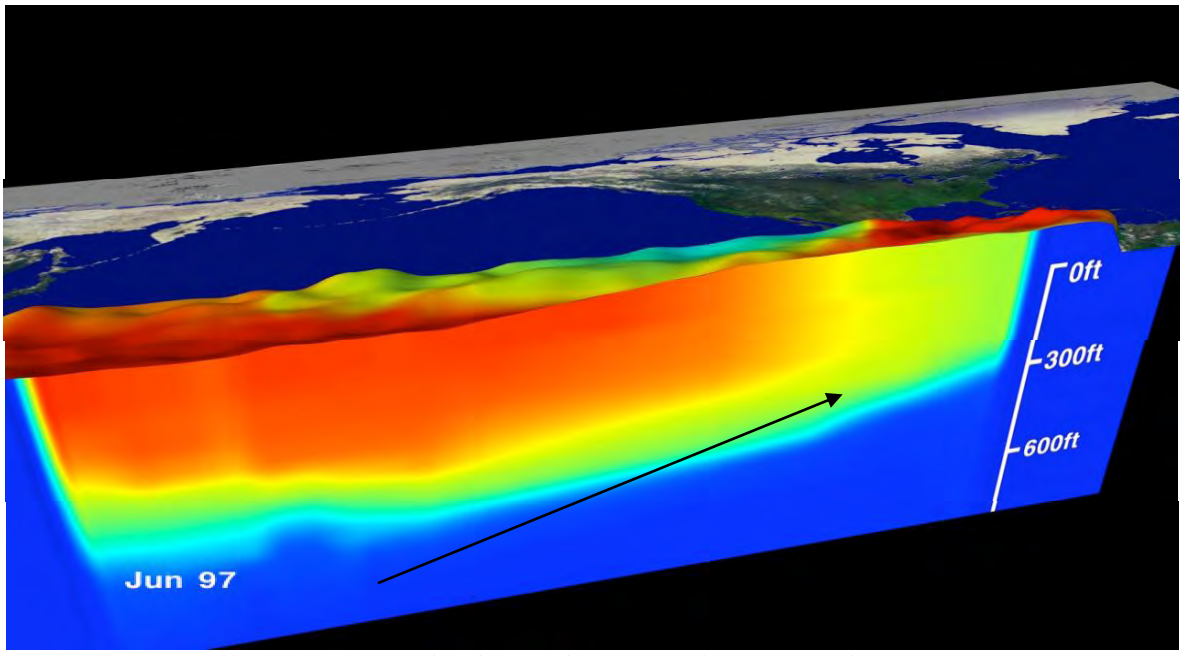

(Source: http://www.usafa.af.mil/dfp/physics/webphysics/jittworkshop/152Sp98GFelNino.html)

Figure 2.6: *cross-sectional view of transition of onset of El Niño condition to full El Niño episode. It shows the critical 1997 El Niño event*.

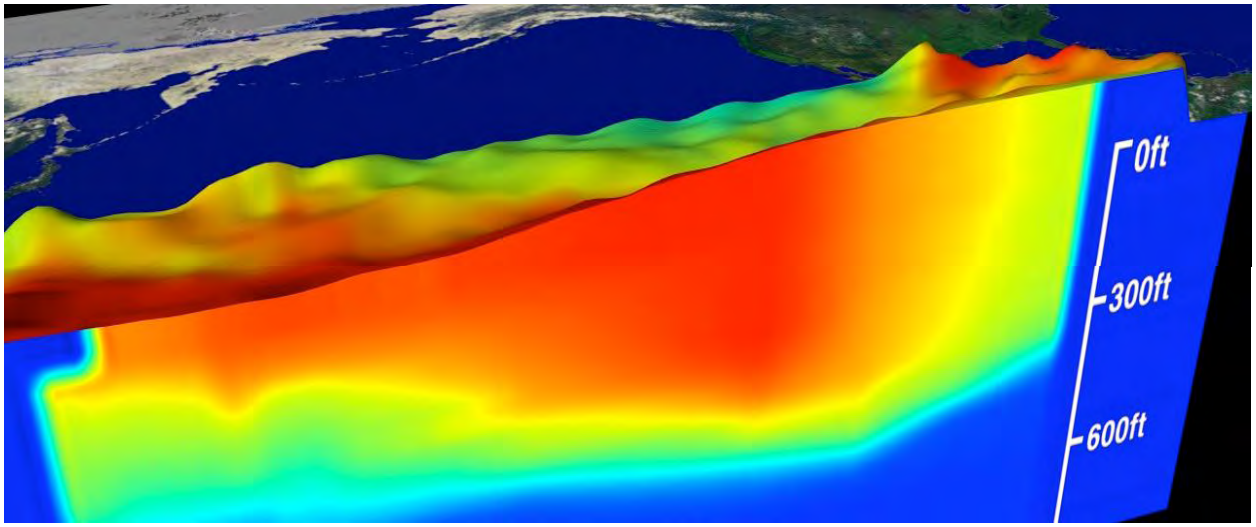

(Source: http://www.usafa.af.mil/dfp/physics/webphysics/jittworkshop/152Sp98GFelNino.html)

Figure 2.7: *Cross-sectional view of full El Niño conditions.*

Thus, more moist air rises along the coast of South America, leading to more clouds and rain than usual. Once the warm water of El Niño hits the coast of South America, it flows north and south along the coast of the Americas, shutting down upwelling and increasing the amount of rainfall. The strongest and most reliable effects take place in the Pacific Ocean near the Equator. The changes that take place there ripple outwards and can affect climate on the other side of the

world. For example, El Niño shifts the position of the Jet Stream, a high altitude air current (–wind"), with important implications for weather throughout the Northern Hemisphere.

In the eastern equatorial Pacific these up well as sea surface temperature (SST) anomalies, which in turn give rise to wind anomalies in the central Pacific. There is a secondary feedback loop in the central Pacific (Wyrtki, 1975; Picaut et al., 1996), whereby SST is affected directly by wind anomalies via advection, anomalous upwelling, evaporation and mixed-layer depth anomalies. These central Pacific SST anomalies in turn influence the wind. The whole system is close to stability and affected by external noise in the form of wind variations. While this conceptual model represents radiative feedbacks (Boer and Yu, 2002) only as damping terms, we should note the climate models examined all have complex representations of clouds and radiation.

Because of the shift of heavy rains to the eastern Pacific, large amounts of latent heat released in thunderstorms should warm the upper troposphere. An upper-level equatorial wind generated through the Hadley cell will transport warm air toward the mid-latitudes. This increase in heat will transfer energy to the jet stream.

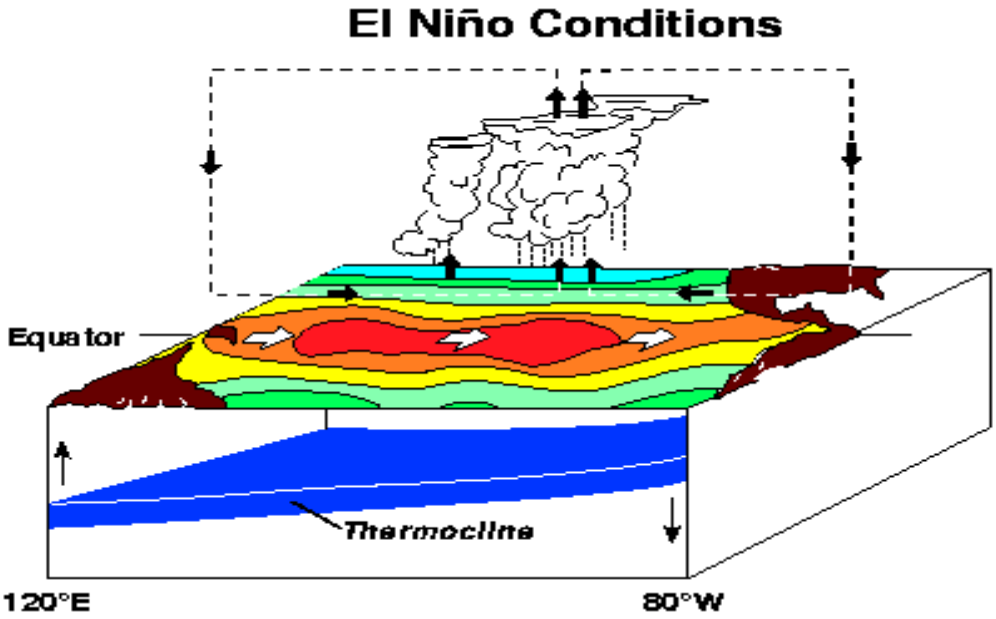

(Source: http://iridl.ldeo.columbia.edu)

Figure 2.8: El Niño conditions, show the relation between ocenic and atmospheric feedback. Arownd 80°W(coast of S.America) thermocline moves down where as 180°E(Indonesia) moves up. Atmospheric feed back clearly shown by dotted line.

After all, the arrival of the Rossby waves near the Asian and Australian continents is marked by a reflection of a second burst of Kelvin waves. The arrival of these waves allows cold water to be

upwelled; easterly winds are re-established signaling an end in the El Niño cycle. SST anomalies decrease and by the following spring, the system is back to normal. (Sirvatka, IRI)

2.3 La Niña phase

Conversely, during La Niño episodes higher than normal pressures are observed over the eastern tropical Pacific and lower than normal pressure is found over Indonesia and northern Australia. And therefore, similar to warm (ENSO) episodes the normal patterns of tropical precipitation and atmospheric circulation become disrupted. The abnormally cool waters in the equatorial central and eastern Pacific give rise to decreased cloudiness and rainfall in that region during winter and spring. Again, mid-latitude synoptic patterns are strongly correlated in cold episodes, although they are not as pronounced as in El Niño events.

La Niña conditions (colder than normal ocean surface temperatures) are good for fishing, but not favorable for farmers, bringing them drought and crop failure.

2.3.1 Normal conditions

Warm sea surface temperatures are common in the western Pacific (Australia, Indonesia, etc.).

Thermocline depth is deep in the Western Pacific and shallow in the Eastern Pacific. Upwelling of cool, nutrient rich ocean water are common in the Eastern Pacific (South America) creating a productive fishery region. Now updrafts and thunderstorms form over the Western Pacific with little activity over the Eastern Pacific.

2.3.2 La Niña Conditions

Cooler sea surface temperatures now move westward as the oceanic wave is reflected off the Southern American Coast. It results thermocline depth becomes very shallow allowing cooler, nutrient ocean water to once again upwell along the South American coast increasing fishery productivity. Convective and thunderstorm genesis once again occurs in the western Pacific. Sub-tropical jet stream is impacted but in contrast to during an El Niño event, the jet stream moves further north cooling and producing more precipitation in the Pacific Northwest and drying the Southwest.

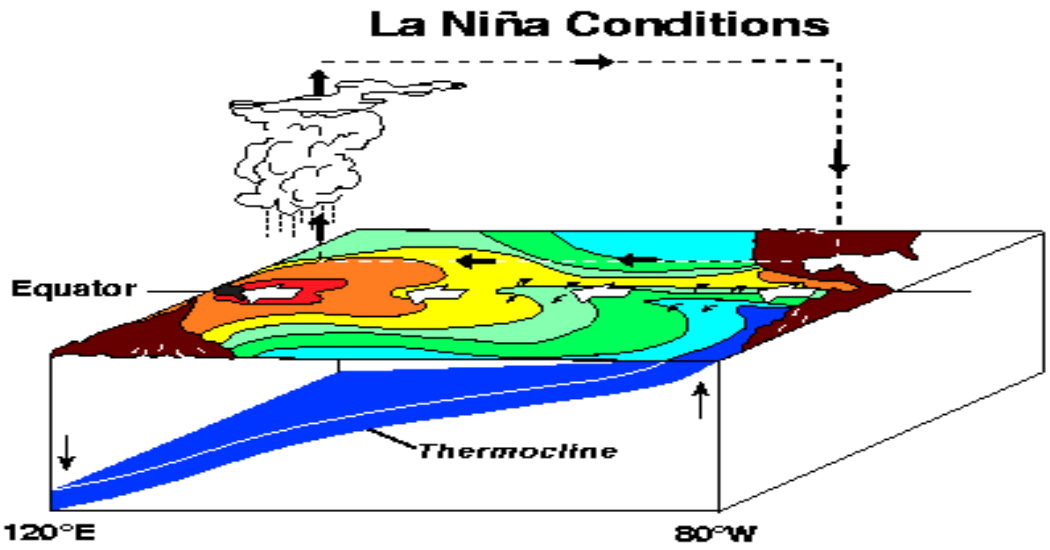

(Source: http://iridl.ldeo.columbia.edu)

Figure 2.9: *La Niña conditions feedback between oceanic and atmospheric circulation*

2.4 El Niño/La Niña Classification

The Oceanic Niño Index or ~~–O~~NI" is commonly used for monitoring, assessing, and predicting of ENSO events. It is based on SST departures from average in the Niño 3.4 region (see Fig. 2.10). The methodology described in Smith and Reynolds (2003) is used to place current conditions in historical perspective. The National Oceanic and Atmospheric Administration (NOAA) operational definitions of El Niño and La Niña are keyed to this index.

A Key to defining the strength of an El Niño/La Niña event is the Sea Surface Temperature Anomalies (SSTA). CPC classifies an El Niño with an anomaly of +0.5^{o}c or higher for 5 consecutive and a La Niña with an anomaly of -0.5^{o}c or lower for 5 consecutive months.

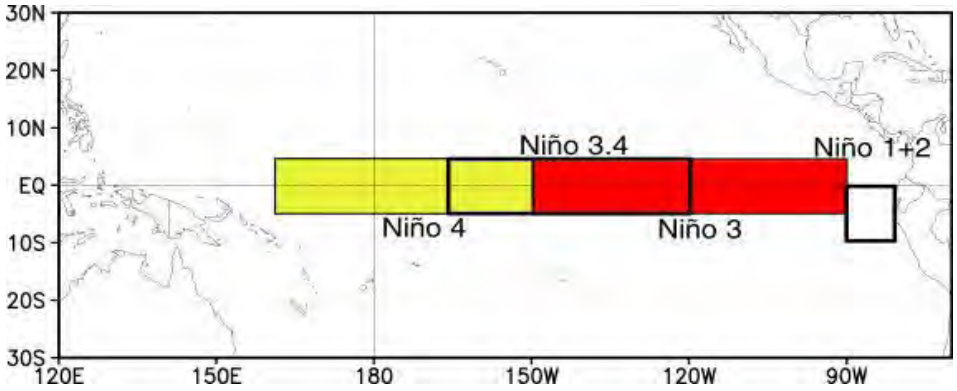

(Source: http://www.cpc.noaa.gov/products/analysis_monitoring/ensostuff/ensoyears.shtml)

Figure 2.10: Location of Niño (El Niño occurred) regions. It's nearly 160^{o}E-90^{o}W and 5^{o}N-5^{o}S

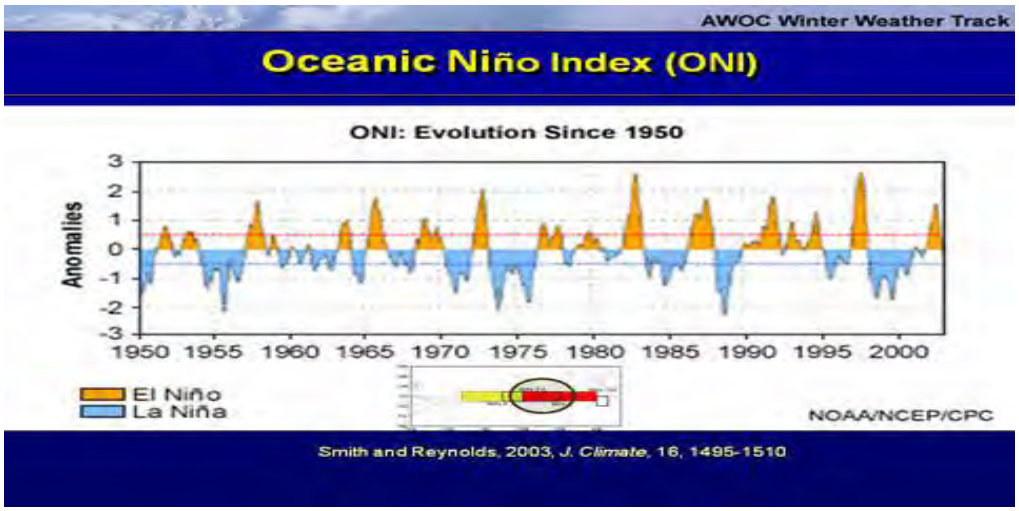

(source: http://www.cpc.noaa.gov/products/analysis_monitoring/ensostuff/ensoyears.shtml)

Figure 2.11*: ENSO episodes based on ONI classification.*

2.5 El Niño/La Niña Jet Stream adjustment

El Niño produces a near horizontal jet stream causing wet conditions in the Southwest. La Niña produces an arching jet stream to the north producing wetter conditions in the Pacific Northwest. Convective circulation by ENSO phenomena, the normal climate pattern will disturb across zonal region, particularly tropical region.

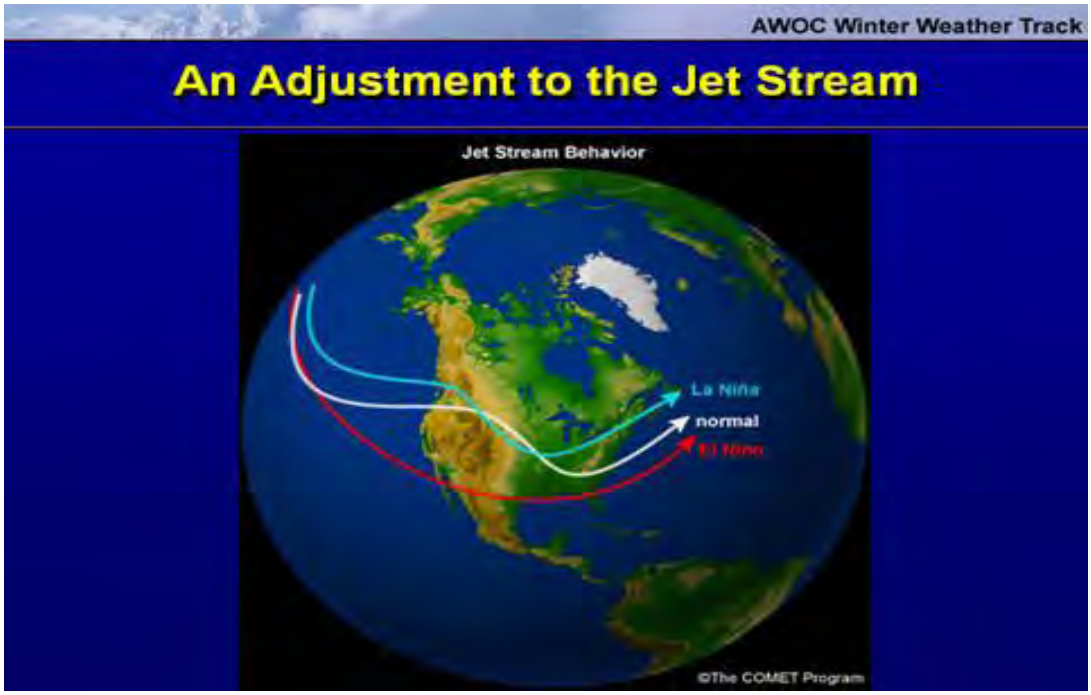

(Source: climate prediction center (CPC), Red for El Niño and Blue for La Niña)

Figure 2.12*: An adjustment of jet streams during ENSO phases relative to the equator.*

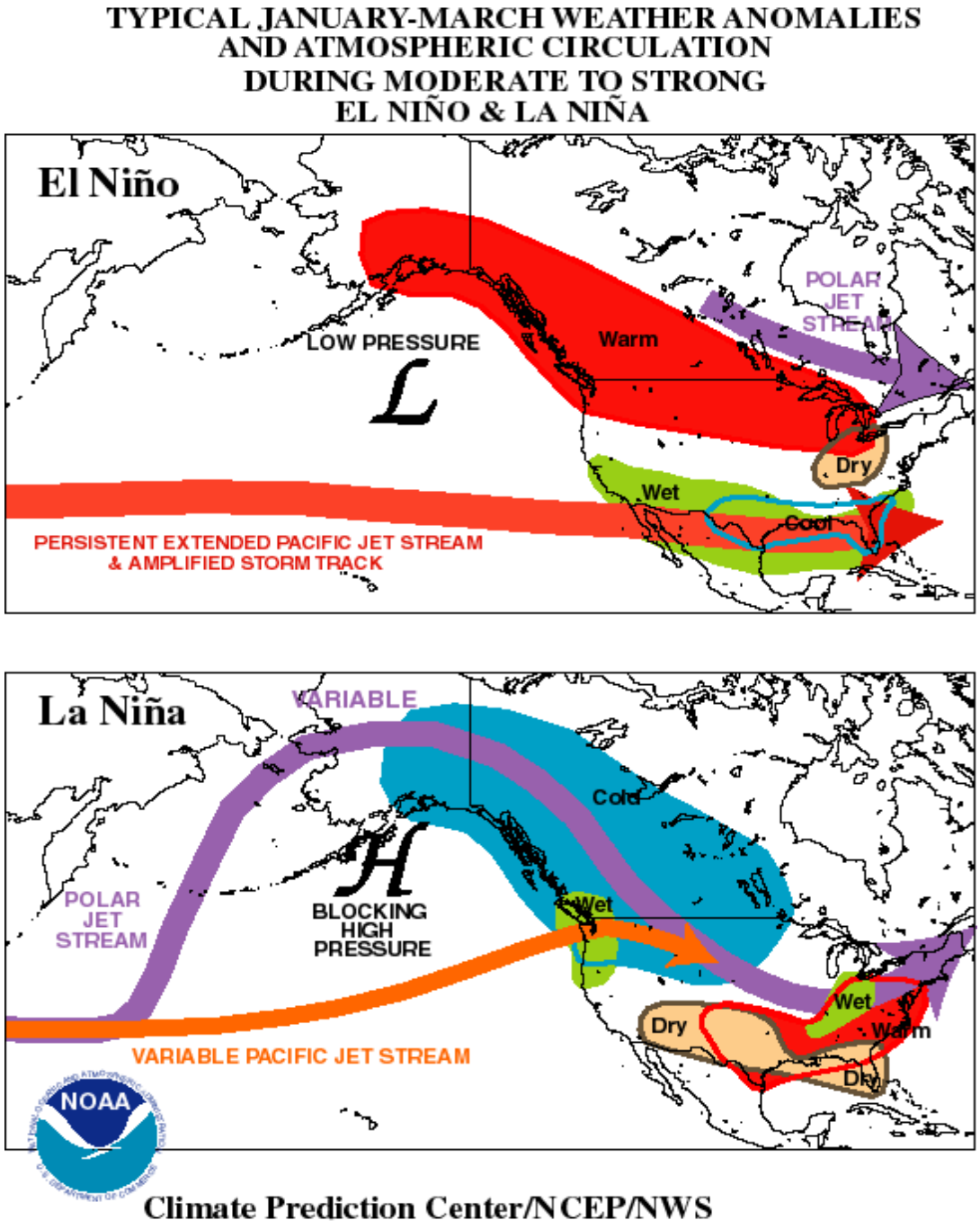

(Source: http://www.cpc.noaa.gov/products/analysis_monitoring/ensostuff/ensoyears.shtml)

Figure 2.13*: The primary atmospheric response to these SST anomalies is an adjustment to the jet stream as the Walker circulation adjusts due to new convective patterns. Convection tends to be longer lived over SSTs of 28°C or greater. Thus a shift in warm SSTs eastward will have a dramatic effect on where convection will be longer lived and hence, adjust the location of the jet stream.*

2.4 The Southern Oscillation (SO)

Sir. Gilbert Walker (http://www.atmos.washington.edu/gcg/RTN/rtnt.html)

It was the atmospheric part of ENSO, i.e. the Southern Oscillation that first attracted the attention of scientists. Sir Gilbert Walker documented and named the SO in the 1930s. The clearest sign of the SO is the inverse relationship between surface air pressures at two sites: Darwin, Australia, and the South Pacific island of Tahiti. So why do we have ENSO? The basic answer is that it appears to be a necessary mechanism for maintaining long-term climate stability (i.e. transport heat from the Tropics to the higher latitudes). El Niño acts to more effectively remove heat from the large tropical Pacific Ocean, and transfer this heat to higher latitudes via the atmospheric circulation. Convection in the tropics is the ~~"b~~ridge" which translates the SST anomalies (El Niño or La Niña) into an atmospheric response, as identified by the Southern Oscillation.

The Southern Oscillation is defined as a "seesaw" in the surface pressure in the South Pacific. Generally over Indonesia and Australia, the pressure is lower than the pressure at Easter Island giving rise to an easterly wind. A reversal in the pressure gives rise to westerly's in the Pacific equatorial zones. The causes for this reversal are not well understood. More specifically, the Southern Oscillation is a coherent pattern of pressure, temperature, and rainfall fluctuations of which the primary manifestation is a "see-saw" in atmospheric pressure between the southeastern Pacific subtropical high and the region of low pressure stretching across the Indian Ocean from Africa to northern Australia (see Fig. 2.14).

The strength of the wind patterns in the Walker Cell can be quantified by the Southern Oscillation Index (SOI). This basically relates the pressure differences between Tahiti and Darwin, Australia. Negative numbers indicate lower pressure in Tahiti and higher pressures in Australia.

$$SOI = Tahiti\ SLP - Darwin\ SLP \qquad (2.1)$$

During El Niño episodes the SOI becomes persistently negative (see Fig., 2.14). Air pressure is higher over Australia and lower over the central Pacific in line with the shift of the Walker Circulation.

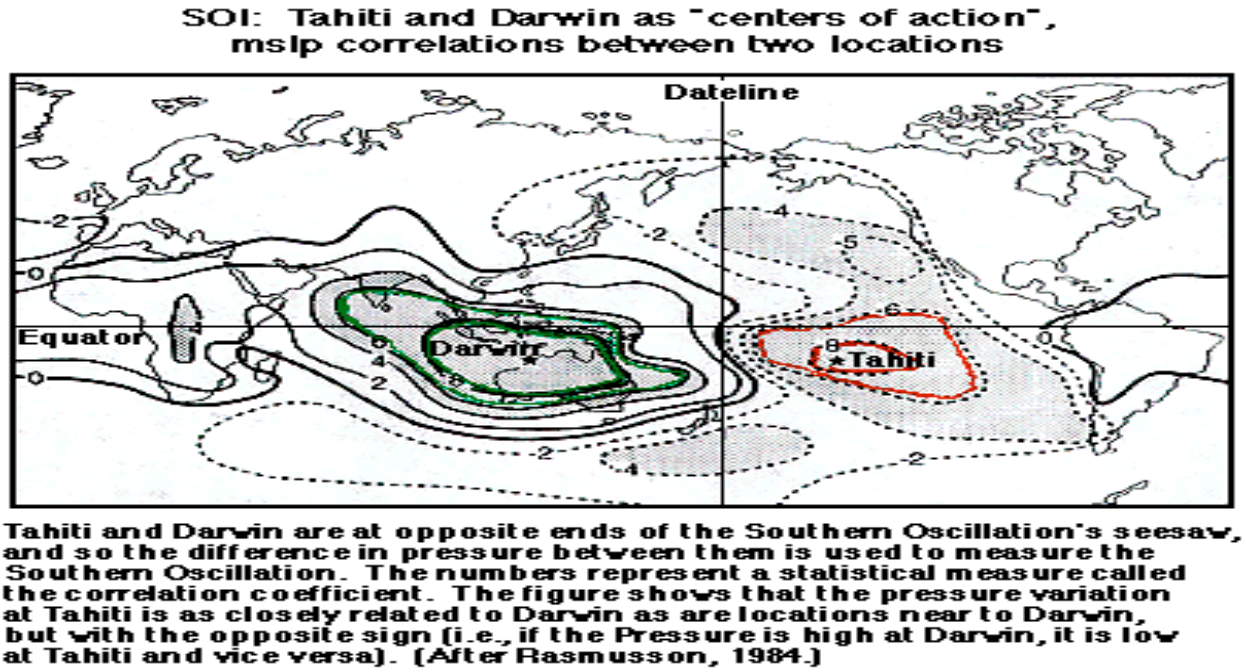

(Source: http://iridl.ldeo.columbia.edu)

Figure 2.14: location of Darwin (Green contour) and Tahiti (Red contour) line

The SOI reflects changes in atmospheric circulation patterns over a wide area and can fluctuate from month to month. Sustained negative values over a period of several months are more usual when an El Niño is developing in the Pacific. Equally, the SOI may occasionally rise close to zero for a month or two during an El Niño event (see Fig., 2.15).

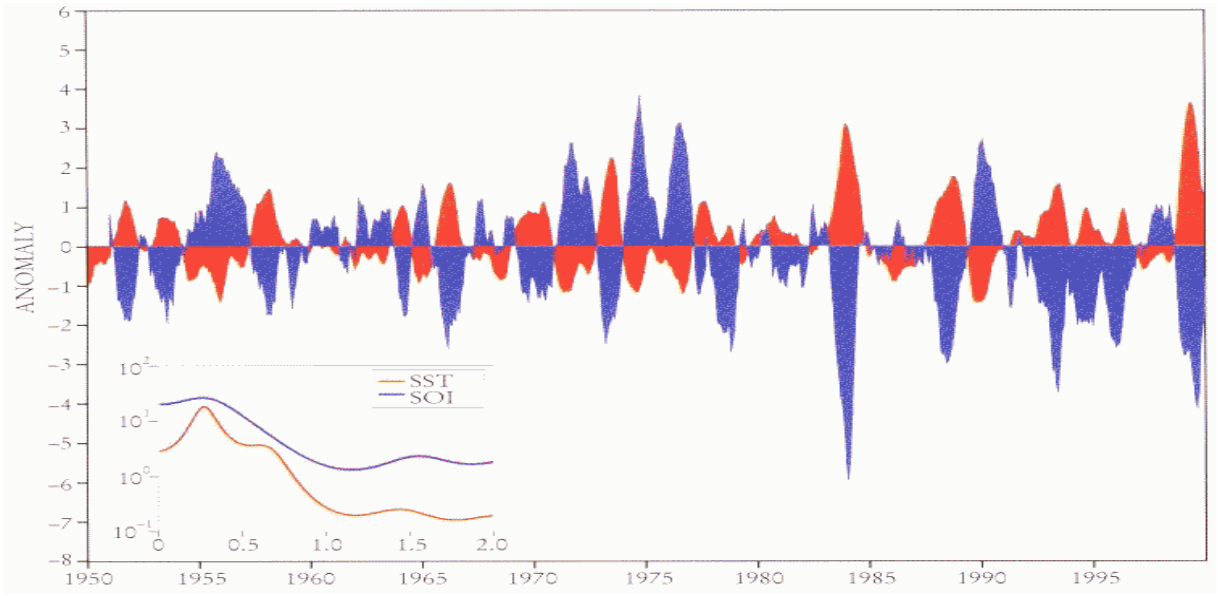

(Source: http://iridl.ldeo.columbia.edu)

Figure 2.15: Correlation between SSTA and SOI.

Fig., 2.15 shows the anticorrelation of the covarying indices of these oscillations [36]. Plotted in red are anomalies (deviations from the long-term mean) of SST averaged over the tropical east-central Pacific. Plotted in blue is the SOI, the normalized pressure difference between Tahiti, in the mid-Pacific, and Darwin, Australia. The SOI measures the pressure gradient across the tropical Pacific which, in turn, is an indicator of equatorial wind variations. When the SOI index reaches low negative values, a strong El Niño is in progress. High positive values indicate La Niña. Power spectra of the covarying time series (inset) show a distinct period at approximately 4 years. The inset axis measures cycles per year.

According to Peixoto and Oort [45] the pressure change comes first, whereas the wind stress lags the SOI by two months. The SST lags it even by 4.5 months. So variations in the pressure gradient, expressed as change in the SOI, are closer to the cause of ENSO events than wind stress and rising sea surface temperature.

El Niño events usually emerge in the period March to June. It is at this time of the year that we can first expect to see the falling of SOI values and the weakening of the Walker Circulation heralding the onset of an event. An event usually reaches its peak late in the year before decaying during the following year.

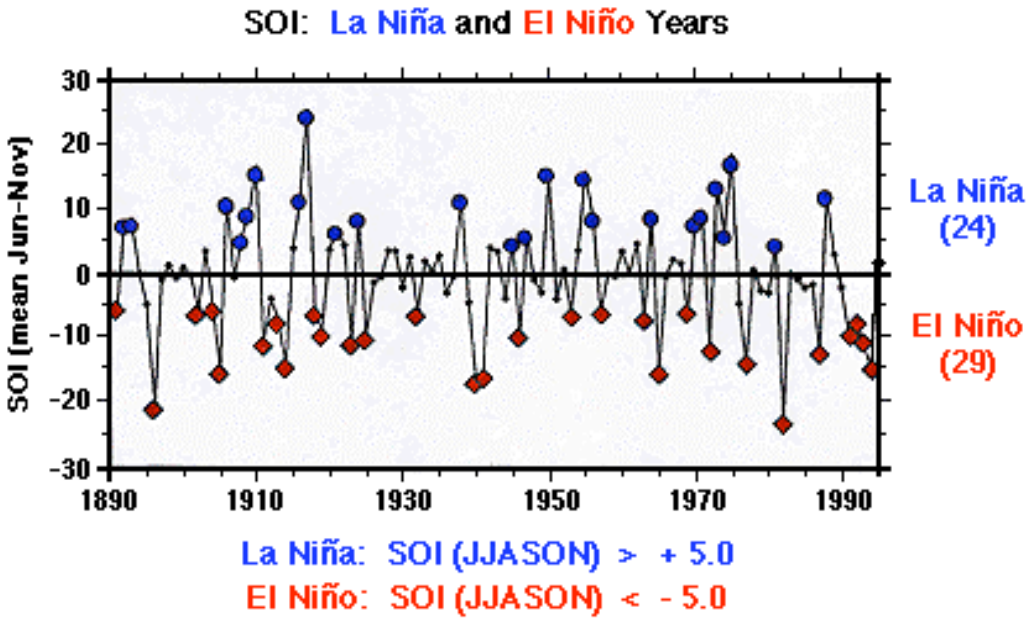

(Source: http://iridl.ldeo.columbia.edu)

Figure 2.16: Relation between SOI, El Niño, and La Niña years

2.7 ENSO and global effect

2.7.1 ENSO model "delay oscillator"

All the above entire complex of atmospheric and oceanic variations are now referred to as ENSO (for El Niño—Southern Oscillation). It is a dramatic example of interannual climate variability associated with atmosphere–ocean coupling.

The leading theoretical model for ENSO is the "delayed oscillator" model. The first successful forecasts of El Niño were made by Mark Cane and Steve Zebiak at Columbia University's Lamont-Doherty Geological Observatory in the US. They developed an intermediate ocean-atmosphere coupled model. The model successfully predicted the onset of the 1986-7 El Niño one year in advance. (Cane et al., 1986; Glebushko, 2004). In this model the sea surface temperature anomaly, T, in the eastern Pacific satisfies an equation of the form

$$\frac{dT}{dt} = bT(t) - cT(t-\tau) \qquad (2.2)$$

where b and c are positive constants and τ is a time delay determined by the adjustment time for the equatorial ocean. The first term on the right represents a positive feedback associated with changes in the Darwin to Tahiti pressure difference. This term represents the atmosphere–ocean coupling through which an initial weakening of the wind causes an increase of the SST, which induces a further weakening of the wind, and hence a further increase in the SST. The second term provides a negative feedback due to the adjustment in the thermocline depth (and hence the ocean temperature) caused by propagating equatorial waves (Rossby and Kelvin) in the ocean that are excited by the SST changes. The time delay in the negative feedback term is determined by the time that it takes for wave energy excited by air–sea interaction in the eastern Pacific to propagate to the western boundary of the ocean, undergo reflection, and propagate back to the region of origin. For realistic parameters the delayed oscillator model leads to ENSO oscillations in the period range of 3–4 years as an average. This highly simplified model qualitatively accounts for the average characteristics of an ENSO cycle, but cannot, however, account for the observed irregularity of ENSO.

In addition to its profound effects in the equatorial region, ENSO is associated with a wide range of interannual climate anomalies in the extra tropics. Thus, the development of models that show skill in predicting ENSO several months in advance is of considerable practical importance (Hortol, 2004).

2.7.2 ENSO on the global effect

The relationship between ENSO events in the tropical Pacific and the seasonal mean surface temperature response over the globe has been extensively documented, both observationally (Kiladas and Diaz 1989, Wolter et. al. 1999) and through model analyses.

In general, ENSO can affect global weather pattern through its teleconnection (Nicholls, and R. Katz, 1991). However significantly affect tropical regions by shifting Jet streams. It also has an effect on global warming. Six months later, after an El Nino phase, the global mean surface air temperature increases. In the tropics and subtropics, this seems to be a consequence of the heat that is given up to the atmosphere as the water cools down in the La Nina phase. After the sever El Nino of 19 97-98 the global temperature went up by over 0.2^{o}C (Trenberth et al. 2002). In tropical area ENSO affects climatic patterns by shifting the Inter Tropical Convergence Zone.

Inter Tropical Convergence Zone (ITCZ)

Inter Tropical Convergence Zone (ITCZ) pronounced ~~–it~~ch" appears as a band of clouds consisting of showers, with occasional thunderstorm, that encircles the globe near the equator (Fig. 2.17). The solid band of clouds may extend for many thousands of miles and is sometimes broken into smaller line segments. The ITCZ follows the sun in that case the position varies seasonally. It moves north in the southern summer and south in the northern winter. The ITCZ is what is responsible for the wet and dry season in the tropics.

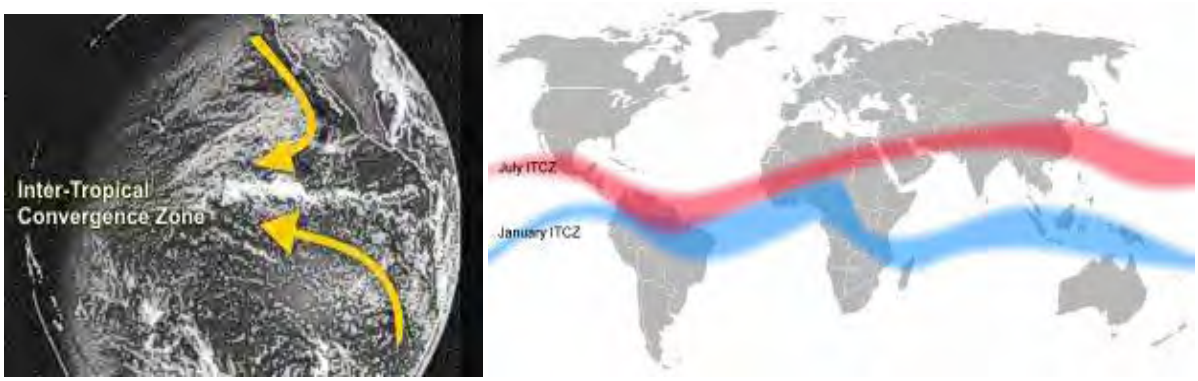

(Sources: National Weather Service, NOAA and
http://en.wikipedia.org/wiki/Wikipedia:Graphic_Lab/Images_to_improve/Archive/Dec_2006#Climate)

Figure 2.17: Location of inter tropical convergence zone. (Left) shows how it will converge in the atmosphere; (Right) shows its location in different season, July (Red) and January (Blue)

ITCZ exists because of the convergence of the trade winds. In the northern hemisphere the trade winds move in a southwesterly direction, while in the southern hemisphere they move northwesterly. The point at which the trade winds converge forces the air up into the atmosphere, forming the ITCZ (National weather service, NOAA). Intense solar heating at the equator causes the sea surface to warm up and the air above to rise there by leaving behind a low-pressure area; the ITCZ, known for centuries by sailors as the *Doldrums*. The rising warm, moist air results in heavy rainfall. The ITCZ appears as a line of deep convective cloud extending across the Atlantic and Pacific oceans between about 5^{o}N and 10^{o}N (*Hasterath*, 1991; *Mitchell and Wallace*, 1992), despite the fact that solar radiation at the top of the atmosphere is nearly symmetric about the equator on annual mean (Hortol, 2004; *Xie,* 2004).

Over the oceans, the ITCZ remains more or less at the equator but over land it moves north and south following the seasonal tilting of the globe towards the sun (Fig. 2.16). Variation in its location results in the alternation of wet and dry seasons in the tropics. Most important, the movement of the ITCZ affects rainfall in southern Africa and the Sahel of western Africa (see Fig. 2.16), particularly vulnerable regions because they have only one rainfall season each year. When the ITCZ does not migrate as far south as usual, droughts can occur in Southern Africa; when it migrates further north than usual it brings heavy rain and floods to the Sahel as happened in 2007(Conway, 2008).Based on the above literature review, ITCZ becomes highly affected by ENSO event.

Unit 3 Ethiopian topographic and climate zones

3.1 Ethiopian topography

Ethiopia with an area of about 1, 000,000 square kilometers is located in the Horn of Africa approximately between 3^{o}N - 15^{o}N latitude and 33^{o}E - 48^{o}E longitude. It is bordered by the Sudan on the west, Kenya on the south, Somalia and Djibouti on the east and Eritrea on the north. It is a mountainous country. The major relief regions of the country influencing the climatic conditions are Western Highlands, Eastern Highlands, the Rift Valley and the Western & Eastern Lowlands. The average altitude of the Western Highland is between 2,400-3,700 meters with the highest mountain Ras Dashen (4620 meters) above sea level, while the Eastern Highland is found in the south eastern part of the country. The Rift Valley is found between these two massifs (Abate and Kefyalew, 1984)

There are numerous mountains and valleys that could in general influence the weather of Ethiopia. It is believed that in the study of weather and climate condition, the relief of Ethiopia will play crucial role. Because of this Ethiopia which is having diverse micro-climates (NMSA, 1996). For the study of climatic conditions of the country data must be collected from different part of the country in such a way that each data point represents homogeneous location.

Figure 3.1a: Location of Ethiopia (blue)

Ethiopia is an agricultural country and its economy is mainly dependent on the rain-fed agriculture. Ethiopia is called the water tower of Africa and the source of many rivers such as the Blue Nile and Wabe Shebelle, making it potentially suitable for irrigated agriculture. The FAO estimates that Ethiopia has the potential to irrigate 3.5 million hectares of land (FAO/GIEWS, 1997). But it has been frequently affected by quasi-periodic drought for a very long time. The failure of seasonal rainfall adversely affects the country‘s socio-economy, in particular food production (Babu, 1999b). To alleviate this problem, a lot of research has been done and results from these studies showed that the major cause of drought in Ethiopia are climate variations across the country especially rainfall variation (Welde-Giorgis, 1997).

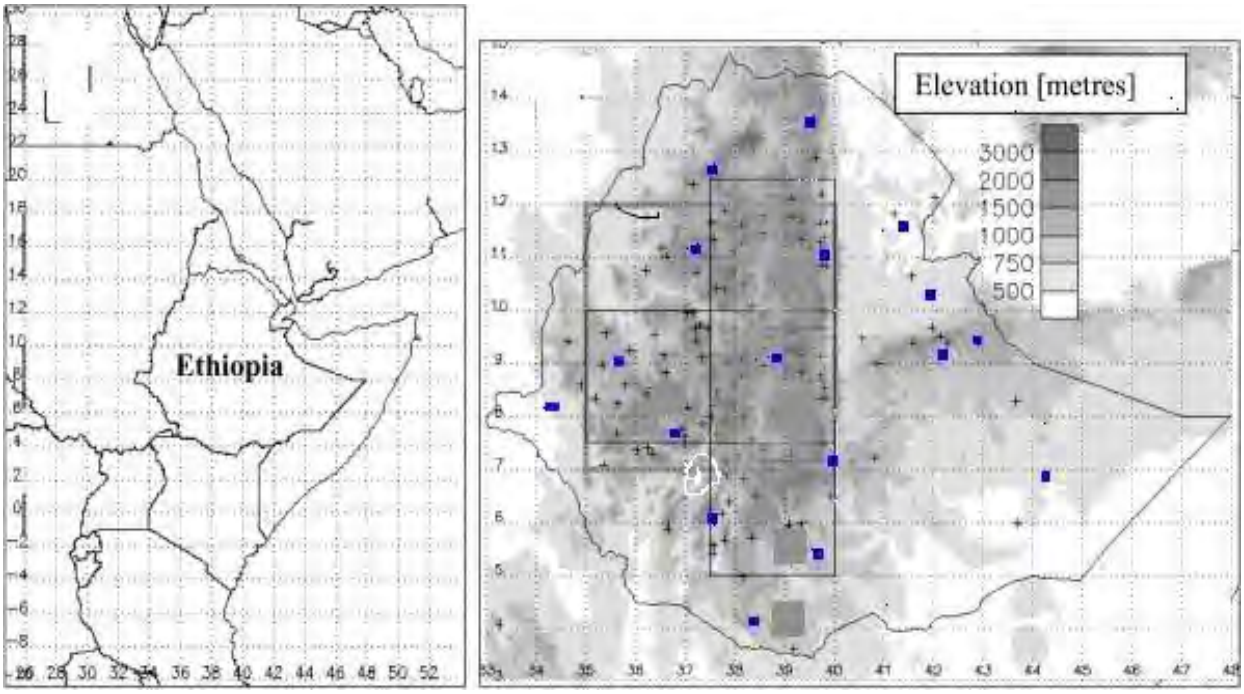

(Source: Dinku, T., et al, 2007-modified)

Figure 3.1b: Representation of the study area of Ethiopian map, blues show locations of data collected regions.

3.2 Seasons and Climate Zones

Understanding the nature of the Ethiopian climate is important for any food security policy in Ethiopia. The Ethiopian National Meteorological Services Agency (NMSA) divides Ethiopia into four climatic zones based on the pattern of rainfall (NMSA 1996). These are:

1. The two-season type: this includes the western half of Ethiopia, which is divided into distinct wet and dry seasons.
2. Bi-two season type: the south and southeastern part of Ethiopia is characterized by double wet seasons. It occurs between March-May and September-November with two dry seasons in between (Workineh, 1987 bibliog.,; Haile 1986 quoted by NMSA 1996).
3. The undefined season mostly has sporadic rainfall between July and February without any defined season. It occurs in the dry northern part of the Ethiopian Rift Valley.
4. The three-season type: these areas include central and southwestern Ethiopia.

The average annual rainfall in the highlands of Ethiopia is above 1000 mm a year and it rises to 2000mm, and 3000 mm in the wet southwestern parts of Ethiopia (NMSA 1996, Babu, 1999a).

The three seasons in Ethiopia are classified according to the amount and timing of rainfall. They are designated as *Kiremt*, (June-September), *Bega* (October-January), and B*elg* (February-May), (NMSA, 1989). These seasons determine the seasonal agricultural activities, such as land preparation, planting, weeding and harvesting by farmers.

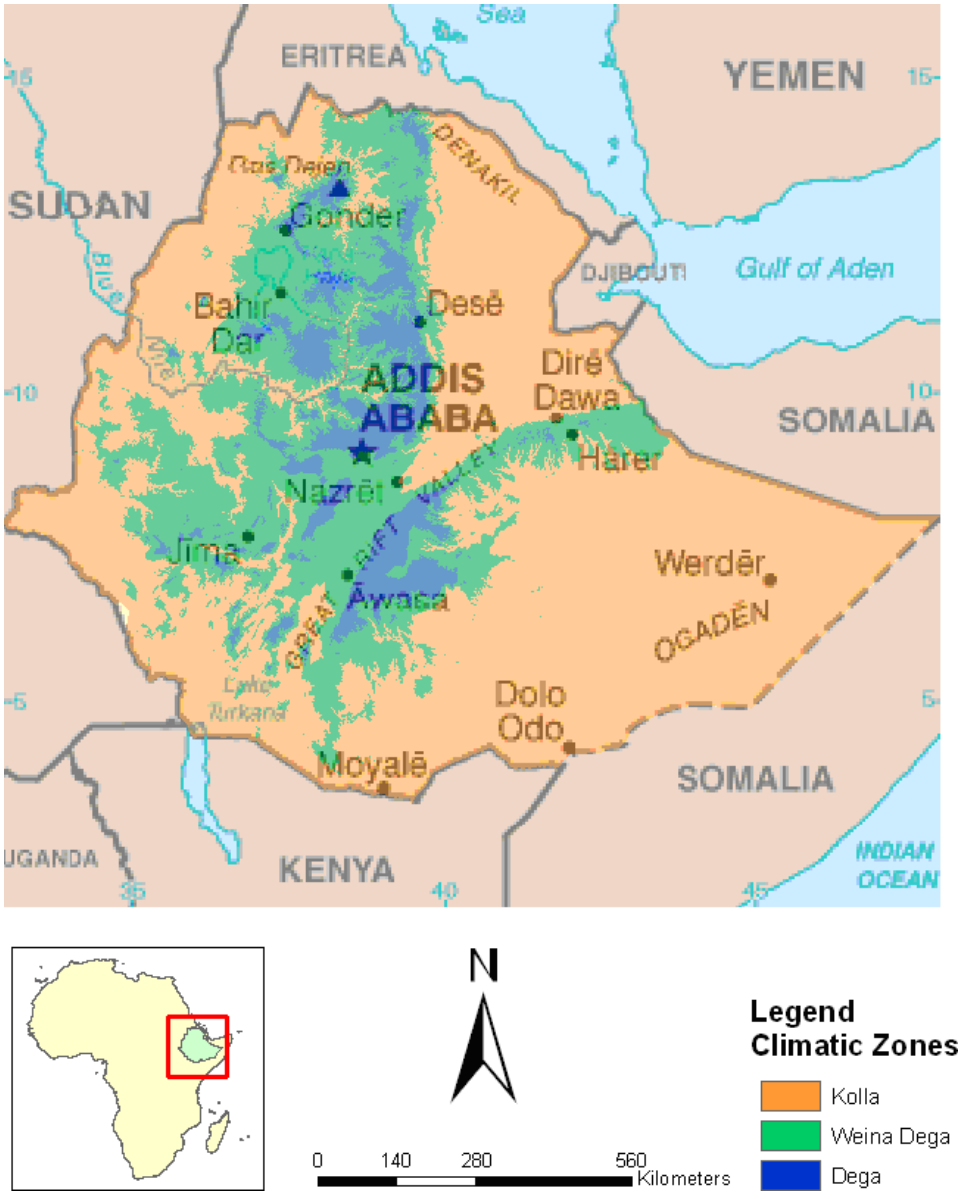

Source: NMSA of Ethiopia

Figure 3.2:major topography and climate regions of Ethiopia.

Kiremt (June-September)

Kiremt is the main rainy season in Ethiopia. There are various regional and global weather systems that affect the *Kiremt* season. These systems include the Inter Tropical Convergence Zone (ITCZ), the Maskaran High Pressure in the Southern Indian Ocean, the Helena High Pressure Zone in the Atlantic, the Congo air Boundary, the Monsoon depression and Monsoon trough, the Monsoon Clusters and the Tropical Easterly Jet (Kassahun, 1999). The ITCZ moves north and south in the tropics following the change of seasons. The ITCZ reaches southern Ethiopia at the beginning of the *Belg season* and moves northward bringing rainfall with it. At the end of August, the ITCZ begins to return southward ending the *Kiremt* precipitation that corresponds with the maturation of crops. Most Ethiopian rainfall, with the exception of the south and southeastern parts of the country, is caused by the ITCZ (Kassahun, 1999).

The High Pressures created in the Makarin and St. Helena areas are important causes for the moisture-carrying wind towards Ethiopia and drop their precipitation in the highlands. The weakening of these high pressures reduces the amount of rainfall in Ethiopia. The Congo Air Boundary in the Congo rain forest is a meeting place for the moisture-carrying winds from the Indian and Atlantic Oceans. This boundary pulls the low air pressure from the north and east into Ethiopia. It also pulls the winds originating from the low pressure in the South Atlantic and provides them with moisture to be dumped in southwestern Ethiopia. Occasionally, the monsoon clusters also provide rainfall to the eastern part of Ethiopia. Finally, the Tropical Easterly Jet, which moves 13 kilometers above sea level over Ethiopia, strengthens the ITCZ, which is the main system that creates rainfall over Ethiopia during the *Kiremt* season (June-September). The absence of this strong wind could negatively affect the amount and distribution of rainfall. The *Meher* crops in the highlands of Ethiopia depend on the *Kiremt* rainfall.

The intensity and fluctuation of the rain-producing systems during the *Kiremt* season influence the amount and distribution of rainfall in Ethiopia (Babu, 1999a). The lack of definition of ITCZ, which is the main rain producing system, causes deficient rainfall over Ethiopia (ibid.). Following Jackson, Abate argues that not all rainfall in Ethiopia is caused by the movement of the ITCZ; other ~~"d~~ry" and ~~"w~~et" periods in Ethiopia are influenced by the atmospheric disturbances that create rainfall away from the ITCZ (Jackson 1979 cited by Abate 1984, pp. 18-19).

Kiremt rainfall is very important in Ethiopia. Most of the food is planted during this season. Drought during *Kiremt* may lead to food insecurity and starvation. With the exception of south and southeastern Ethiopia, most parts of the country receive 60 to 90 percent of their rainfall during the *Kiremt* season (Babu, 1999a).

Bega (October-January)

The B*ega* season occurs between October-January. *Bega* is the dry, windy and sunny season in most highlands of Ethiopia. The causes of this dry season are the Sahara and Siberian High Pressure that send dry and cold winds to Ethiopia during the northern winter (Kassahun, 1999). During the B*ega*, most of highland Ethiopia is sunny during the day and cold during the night and morning, which includes frost in December and January. Farmers harvest their *Meher* crops during this dry period. However, there are some areas of lowland Ethiopia, such as the Ogaden, which get some rainfall during this period.

A low pressure air that moves from Western to Eastern Europe, occasionally, passes over Ethiopia and interacts with warm and humid air from the tropics creating unseasonable rainfall in Ethiopia during the B*ega* (Kassahun, 1999). Moreover, the tropical disturbances on the Arabian Sea might move to Ethiopia and drop some rainfall during the B*ega* season, especially in the pastoral areas of the country. The pastoral areas of south and southeastern Ethiopia experience a bi-modal rainfall regime and receive their rainfall between October-January and February-May.

The precipitation during the B*ega* season (October –January) is generally very low in most of the grain-producing parts of Ethiopia. However, the regions in southern, southwestern and southeastern Ethiopia receive rainfall associated with the southward retreat of the ITCZ (Babu, 1999). By the end of November, dry Arabian and Saharan anticyclones replace the Southward shifting ITCZ and bring warm-dry weather to Ethiopia. At times this new air Circulation meets with tropical air masses and brings untimely and unwanted rainfall to Ethiopia. The wind direction also reverses from wet westerlies to dry easterlies that bring dry and cold wind to Ethiopia. Rainfall in Ethiopia decreases from SW to NE.

Belg (February-May)

The *Belg season* is also known as the small rain period and occurs between February-May. The *Belg rains* begin when the Saharan and Siberian High Pressures are weakened and various atmospheric activities occur around the Horn of Africa. Low-pressure air related to the Mediterranean Sea moves and interacts with the tropical moisture and may bring precipitation to the region. The high pressure in the Arabian Desert also pushes that low-pressure air from south Arabian Sea into mid- and southeast Ethiopia, which in turn, creates the *Belg rains*. The beginning of the *Belg rain* is also the period when the ITCZ begins to reach south and southwest Ethiopia in its south-north movement (Kassahun, 1999). The *Belg rains* fail when these diverse weather phenomena are not realized. For example, the creation of strong low pressure and cyclones in the southern Indian Ocean reduces the amount and distribution of rainfall in Ethiopia.

Between 5 and 10 percent of crops in Ethiopia are produced during the *Belg season*. In some areas, the *Belg* rainfall may produce up-to fifty per-cent of local food. The small rains also contribute to increased pasture for domestic and wild animals. Normal *Belg rainfall* adds moisture to the soil, easing land preparation for the *Kiremt* planting. During the dry season, the mass of dry air comes from the northeast. (Abate, 1984)

The *Belg season* is influenced by the tropical surface air masses in the Indian and Arabian anticyclones and the Central African cyclones south of Ethiopia (Haile, 1987). At the beginning of March, the ITCZ arrives in southwestern Ethiopia to move northward which brings rainfall (Babu, 1999a). *Belg rainfall* is brought by the penetration of extra-tropical troughs that replace the Arabian anticyclones (Babu, 1999). The *Belg* rains normally end in the middle of May and dry weather persists (for a month) until the middle of June when the *Kiremt* wet season begins. Babu (1999a) argues that the *Belg* rains may sometimes merge with the *Kiremt* rainy season without the one-month break. He states, "Merging *belg* and *Kiremt* rains was observed in 1972, 1977, 1982, 1987 and 1993, which were all El Niño years. So the presence or absence of El-Nino could be used as a predictor to anticipate *Belg* or *Kiremt* rainfall" (Babu, 1999).

Microclimates in Ethiopia

In addition to the ITCZ, local factors also affect rainfall in Ethiopia. Spatial variations caused by altitude create rainfall variations in Ethiopia leading to the existence of various microclimates. Altitude is an important factor in creating various climatic zones in Ethiopia. The four types of climate zones in Ethiopia are the *Dega, Weina-dega, Kola* and *Bereha*. The *Dega* is cool and usually receives adequate rainfall. The *Weina- dega* is temperate and supports most Ethiopian crops. The *Kola* is hot and includes the lowland areas. The *Bereha* is the desert type area in the peripheral parts of the country in which nomadism is the main economic activity (Babu, 1999a)

The major Rainfall seasons in Ethiopia are largely the result of the migration of ITCZ. Findings show that ITCZ is highly sensitive to ENSO. The National Meteorological Service Agency (NMSA) of Ethiopia believed that, ENSO is strongly related to rainfall distribution in the different parts of the country (Babu, 1999b). Researchers at NMSA and policy makers in Ethiopia believe that the state of SSTs in the tropical Pacific Ocean affect Ethiopian climate through teleconnections (Haile, 1988). The disturbance of ITCZ results the country insufficient food production and drought across the country (Welde-Giorgis, 1997). NMSA also believes that the Atlantic and the Indian oceans' SST anomalies also affect Ethiopia. Other studies also support the NMSA's conclusions. For example, the variability between high and low flood levels of the Nile River, whose major water source is highland Ethiopia, is related to the ENSO cycle (Quinn, 1992).

Based on the fact as we discussed in the above units of literature reviews, all these research missed scientific facts of microclimate zones of the country, seasonal variations of rainfall,

quasi- periodic nature of ENSO and wave disturbances of ocean-atmospheric couple system or ―see-saw" nature. Based on these scientific facts this paper considers the following points:

- Data taken long period of time 1962 to 2005 except satellite data started 1979 for seven locations.
- Missed data filled with a systematic mathematical analysis from satellite.
- Both data were taken as SSTA and RFA with scientific methods of selecting ENSO event only.
- Correlation analyses with time lag for each micro-climate zone determine. Finally the detail analysis of the result found by using Spectrum analysis.

All these scientific reasons and facts are briefly discussed in the next unit.

Unit 4

Data and data analysis

4.1 Data sources

The rainfall data used in this work emanate from the NMSA of Ethiopia and partially satellite data from the National Oceanographic and Atmospheric Administration Climate Prediction Center (NOAA-CPC) merged analysis (CMAP) (xie et al. 2003). This data contains long period of time and is more appropriate for Ethiopian rainfall estimation (Dinku et al. 2007). Data were taken mean monthly rainfall from 1962 – 2005 from the NMSA and satellite data taken from 1979-2005. Systematic selections of 17 stations were based on their locations in the diverse microclimate zones and the size of the data become large enough to provide a precise estimation of the effect (see Fig., 3.1b). Initially ten stations data from NMSA results unsatisfactory so an additional seven stations are added from satellite like Arba- Minch, Asaita, Gambela, Harar, Kebri-Dar, Mega and Shinile.

The second category of data for this paper was sea surface temperature anomaly (SSTA) across the pacific area. The influential location for ENSO phase can be considered as Nino region. In general the region as already been indicated in Fig. 2.9 covers the area 5^oS-5^oN and 160^oE-90^oW (Boer, and Yu, 2002). SSTA data was taken from the National Climate Data Center (NCDC). The data spans the time from 1962 to 2005 and it is taken from the location 2^oS and 240^oE (120^oW) where ENSO effect is observed or Nino 3.4 region. ENSO phases occur when SSTA ranging above $+0.5^oc$ and below -0.5^oc for five consecutive months (CPC classification, see Fig., 2.10 &2.11).

4.2 Data processing methods

4.2.1 Interpolation and Selecting data from complex effects

Since the measured rainfall data set begins at different time series, it had to be extrapolated into similar time series using information from satellite. Then mean monthly rainfall for each location has been derived. Finally the mean value from each monthly data was subtracted. This gave us rainfall anomaly (RFA) for each location, which is readily compared with SSTA. The SSTA data was calculated with a similar fashion as that of RFA. The main reason for this calculation is to determine ENSO events predicted by CPC (Boer, and Yu, 2002).

One of the major problems in processing the rainfall data was the missing values. In some locations except Addis Ababa, Bahir-Dar and Combolcha all are missed for longer period and frequently. Processing the raw data would have a significant effect on the result. The first step was to interpolate the missed data. For this purpose a trend analysis has been done to determine

the scaling factor so that missed rain gauge data can be interpolated from satellite data. Mathematical equations of trend analysis with best fitted are found in Appendix A. Direct merging of satellite data with the missed gauge data was impossible for mountainous and equatorial regions (Dinku et al., 2007). That is why careful trend analysis was needed for each location.

The above rain gauge data is influenced by many factors such as seasonal variations and some unknown factors (considered as noise). Since the aim of this work is to study the effect of ENSO on the Ethiopian rainfall pattern it was necessary to window both data set in ENSO window using filtering technique in the spectral domain. Previous research showed that ENSO occurs at an average of every 3 to 4 years but over a period which varies from 3 to 7 years, and is therefore, widely and significantly, known as "*quasi-periodic*". Therefore both data sets were filtered with band pass filter with period of 3 to 7 years.

4.2.2 Fourier series for data processing

In the perturbation method, all field variables are divided into two parts, a *basic state* portion, which is usually assumed to be independent of time and longitude, and a perturbation portion, which is the local deviation of the field from the basic state. Thus, for example, if T_o designates a time and longitude-averaged zonal *temperature* and T is the deviation from that average, then the complete zonal temperature field is

$$T(x,t) = T_o + T'(x,t) \qquad (4.1)$$

The representation of a perturbation as a simple sinusoidal wave might seem an oversimplification since disturbances in the atmosphere are never purely sinusoidal. It can be shown, however, that any reasonably well-behaved function of longitude can be represented in terms of a zonal mean plus a *Fourier* series of sinusoidal components (T)(Hortol, 2004).

$$T(x,t) = T_0 + \sum_{-\infty}^{\infty} \left(a_n \cos \mathrm{n}\pi\left(\frac{x}{L} - \frac{\mathrm{t}}{\mathrm{T}}\right) + b_n \sin \mathrm{n}\pi\left(\frac{x}{L} - \frac{\mathrm{t}}{\mathrm{T}}\right)\right) \qquad (4.2)$$

Taking the deviation of eqn. (4.2), we can get anomaly function. This anomaly function is a Fourier series function, Symmetry about the x-axis:

$$T(x,t) - T_0 = \sum_{-\infty}^{\infty} \left(a_n \cos \mathrm{n}\pi\left(\frac{x}{L} - \frac{\mathrm{t}}{\mathrm{T}}\right) + b_n \sin \mathrm{n}\pi\left(\frac{x}{L} - \frac{\mathrm{t}}{\mathrm{T}}\right)\right) = T' \qquad (4.3)$$

Based on eqn. (4.3), CPC uses ENSO prediction based on disturbance of ocean-atmospheric waves and Sea Surface Temperature Anomaly (SSTA). Using properties of Fourier functions, it‘s possible to perform data analysis system to get a significant effect of ENSO.

In the filtering procedure one should ascertain that information within the quasi-periodic intervals of ENSO is preserved. The approach used in this work is to transform the data to frequency domain and suppress all data out of the selected periods.

In the Fast Fourier Transform (FFT) filtering data in the time domains is first transformed into the frequency domains and later the frequency range of ENSO occurrence (0.143 to 0.333 cycles per year) was used as the cut off frequency for the band pass filter of Butterworth.

The software used for this purpose was ORIGIN PRO 8 (http://www.origin.com).

The removal of frequencies is strictly limited to known effects (e.g., McCarthy and petit, 2004, pages 93-94). After completing the frequency domain filtering the data was transformed back to time domain using the Inverse Fast Fourier transform (IFFT). This will in principle transform the FFT result back to its original data set. The resulting filtered data is given together with the raw data in Fig. 4.1.

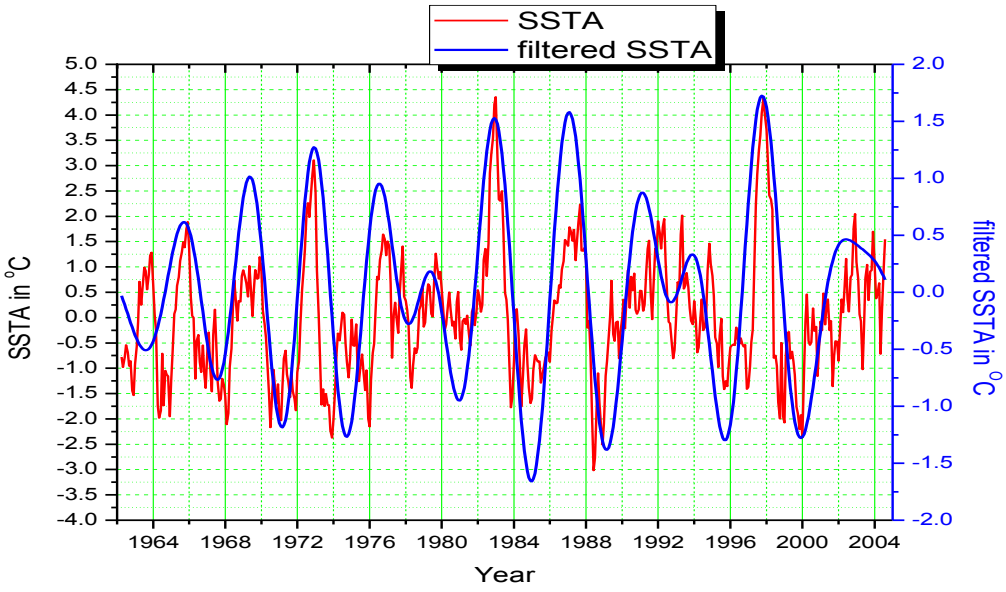

Figure 4.1 Relation between SSTA and filtered SSTA

In a similar fashion all RFA data sets are filtered using the same cutoff frequencies. Through this approach it is believed that effects only within ENSO period are kept in both data sets.

4.2.3 Correlation analysis: time domain

Auto- covariance function/auto-correlation

Definition: Let $x(t)$ be a real or complex valued stationery process with mean $\bar{x}$ then

$$\rho(\tau) = \varepsilon(\,(x(t) - \bar{x})(x(t+\tau) - \bar{x})^{*}\,) \qquad (4.4)$$

$$= Cov\,(x(t), x(t+\tau))$$

is called the auto -covariance function of $x(t)$, and the normalized function

$$r(\tau) = \frac{\rho(\tau)}{\rho(0)} \qquad (4.5)$$

is called the auto – correlation function of $x(t)$. The argument τ is called the *lag*. Note that the auto correlation and auto covariance functions have the same shape but they differ in their units. $\rho(\tau)$ has units of x^2 where as $r(\tau)$ is dimensionless. When required for clarity, we will identify the auto-covariance and auto- correlation function of process $x(t)$ as ρ_{xx} and r_{xx} respectively.

The auto-correlation function can be interpreted as an indication of the skillfulness of the persistence forecast of $x(t+\tau)$ that is constructed when an observation $x(t)$ is ‗persisted' τ time steps into the future. In this context $r(\tau)$ is the correlation between the forecast made at time t and the verifying realization that is obtained after τ time steps later. The portion of variance ‗explained' by the persistence forecast is $r^2(\tau)$.

For complex valued process, for convenience, assume that $x(t)$ has mean zero (as perturbing term). Note that we may express the auto-covariance function, eqn. (4.4) as polar coordinates

$$\rho(\tau) = \boldsymbol{\varepsilon}\,(\,x(t), x(t+\tau)^{*}) = A(\tau)e^{-i\varphi(\tau)} \qquad (4.6)$$

where A (τ) and φ (τ) are the amplitude and phase functions of lag τ. Auto-correlation function is symmetric about the origin,

$$r(\tau) = r(-\tau)\,, \qquad (4.7)$$

and that it does not take values outside the interval [-1,1](if x is real) or outside the unit circle(if x is complex). That is $|r(\tau)| \leq 1$ (4.8)

(Storch, and Zwiers, 1999, p.217-280).

Cross-covariance/cross-correlation

Definition: let $(x(t), y(t))$ represent a pair of stochastic process that are jointly weakly stationary. Then the cross –covariance function ρ_{xy} is given by

$$\rho_{xy}(t) = \varepsilon\big((x(t) - \bar{x})(y(t) - \bar{y})^*\big) \quad (4.9)$$

The cross- correlation function r_{xy} is the normalized cross- covariance function.

$$r_{xy}(\tau) = \frac{\rho_{xy}(\tau)}{\sqrt{\rho_{xx}(0)\rho_{yy}(0)}} \quad (4.10)$$

where $(\rho_{xx}(0))^{1/2}$ and $(\rho_{yy}(0))^{1/2}$ are the standard deviations of processes x and y respectively. The detail explanation was given by Pearson correlation in the following paragraph for SSTA and RFA.

Each rainfall data (RFA) checked whether there is a relationship between SSTA or not. The Pearson correlation coefficient is computed to study the interaction between them. These tests are useful in determining the strength and direction of the association between two scale or ordinal variables. By definition the Pearson correlation coefficient between two time series x and y, at a time lag of τ, is computed as $r(\tau)$, using

$$r(\tau) = \frac{\sum_i [x(i) - \bar{x}] * [y(i+\tau) - \bar{y}]}{\sqrt{\sum_i [x(i) - \bar{x}]^2} * \sqrt{\sum_i [y(i+\tau) - \bar{y}]^2}} \quad (4.11)$$

Here $\bar{x}$ and $\bar{y}$ are means of corresponding series of x and y, with $i = 1, 2, 3, \ldots, N$ being the i^{th} data point in each series and N is the total number of data points. It should be kept in mind that data is cyclic and hence data wrapping has been applied.

4.2.3 Spectrum analysis: frequency domain

It is a common practice to counter check the result found in the time domain and analyzes it further in the frequency domain, through the use of spectrum analysis. The usage of spectrum analysis will not only allow to study the correlation and time lag between ENSO and Rainfall, but also analyzes which frequency bands are responsible for the correlation at a given phase lag.

Power spectrum and cross power spectrum

Definition of power spectrum ($s_{xx}(\omega)$ *or* $s_{yy}(\omega)$)

The spectrum (or power spectrum) S of $x(t)$ is the Fourier transform $\mathcal{F}$ of the auto-covariance function ρ. That is

$$S(\omega) = \mathcal{F}\{\rho\}(\omega) = \sum_{-\infty}^{\infty} \rho(\tau) e^{-2\pi i \tau \omega} \qquad (4.12)$$

for all $\omega \in [-1/2, 1/2]$.

Note also that the spectrum and the auto-covariance functions are parameters of the stochastic process $x(t)$.when the process parameters are known (not estimated from data), the spectrum is well-defined and not contaminated by any uncertainty.

Definition of cross spectrum

Let $x(t)$ and $y(t)$ be two weakly stationary stochastic process with auto-covariance functions ρ_{xx} and ρ_{yy} , and a cross-covariance function ρ_{xy} . Then the cross-spectrum $s_{xy}(\omega)$ is defined as the Fourier transform of ρ_{xy} .

$$S_{xy}(\omega) = \mathcal{F}\{\rho_{xy}\}(\omega) = \sum_{-\infty}^{\infty} \rho_{xy}(\tau) e^{-2\pi i \tau \omega} \qquad (4.13)$$

for all $\omega \in [-1/2, 1/2]$.

For any two random time series $x(t)$ and $y(t)$, their power spectrum are $s_{xx}(\omega)$ and $s_{yy}(\omega)$ respectively and their cross-power spectrum is $S_{xy}(\omega)$. The complex coherence function $c_{xy}(\omega)$ is computed using,

$$C_{xy}(\omega) = \frac{s_{xy}(\omega)}{\left(s_{xx}(\omega) s_{yy}(\omega)\right)^{1/2}} \qquad (4.14)$$

Here ω is the frequency. Since $s_{xx}(\omega)$ and $s_{yy}(\omega)$ are real quantities and $S_{xy}(\omega)$ is complex, it automatically follows that $c_{xy}(\omega)$ will be a complex quantity with magnitude and argument. The magnitude $(0 < \gamma(\omega) < 1)$ is called the coefficient of coherence (Foster and Guinzy, 1967) and the argument $(-\pi < \varphi(\omega) < \pi)$ is the phase lag.

Essentially, γ is the average, normalized amplitude of the cross power spectrum. It is the measure of how good the two time series are correlated. It is mathematically analogue to the Pearson product moment correlation given equation (4.11). The square of $\gamma(\omega)$ equation (4.15) is the squared coherence spectrum, which also satisfies the inequality $0 < \gamma^2(\omega) < 1$ (Jenkins and

Watts, 1968). In some literature the square coherence is referred to as the coherence function (e.g., Otens and Loren, 1972). In this paper we preferred to call $c_{xy}(\omega)$ in equation (4.14) as the complex coherence function, its magnitude $\left|C_{xy}(\omega)\right|$ the coefficient of coherence and $\gamma^2(\omega)$ in equation (4.15) as squared coherence spectrum:

$$\gamma^2 = \left|\mathrm{C_{xy}}(\omega)\right|^2 = \frac{\left|\mathrm{S_{xy}}(\omega)\right|^2}{\mathrm{S_{xx}}(\omega)\mathrm{S}_{yy}} \qquad (4.15)$$

The direct application of equation (4.15) on linearly dependent data will give unity at all frequencies, irrespective of what the true values are. To overcome this problem one can either averaging $S_{xx}(\omega), S_{yy}$ and $S_{xy}(\omega)$, over adjacent frequencies or average the replications of data at a given frequency, from different realizations, or combine both approaches. In this work, both approaches are used together. Actually, by averaging the power spectrum based on sampled data we are trying to approximate equation (4.15) and hence, in practice, we are computing the squared sample coherence $\gamma^2(\omega)$. However, for the purpose of simplicity we will refer to this quantity as squared coherence. Since the process of averaging stabilizes the coherence value but degrades the spectral resolution the choice of the windows has been done carefully not to lose too much resolution (Lewi and Groten, 2005).

The replication of data at a given frequency is usually attained by dividing each data into k blocks and compute $S_{xx}{}^j(\omega)$, $S_{yy}{}^j(\omega)$, and $S_{xy}{}^j(\omega)$, *for j = 1, 2, ..., k*. Here we have used Welch Modified periodogram method (Welch, 1967; Rabiner and Gold, 1975) to generate the different blocks, in this method; any two time series (in our case SSTA and RFA) will be segmented into k blocks, with the same amount of data that have overlapping data points. Then the mean values $\hat{s}_{xx}$, $\hat{s}_{yy}$ and $\hat{s}_{xy}$ at the frequency ω, are obtained by averaging the data from the k blocks. Using these averaged power and cross power spectral densities, spectral averaging over adjacent m discrete frequencies has been carried out by averaging the cross- power spectrums within the given frequency window.

The coherence value achieved using the above procedure should judge for its reliability, so that it can be accepted as a reasonable estimate. For this the measure given in equation (4.16) has been used (Brillinger, 1975, p.334).

$$C^2 = 1 - \alpha^{1/(n-1)} \qquad (4.16)$$

where α = 1-p and p*100% is the confidence threshold. In some literature (e.g. Thompson, 1997) equation (4.16) is used with n=k, where k is again the number of realizations or the number of data blocks. Others (e.g., Chao, 1988) use n=m, which is the number of elementary Fourier bandwidth, where spectral averaging is conducted. Here we used equation (4.16) with n= m + k, where m and k have the same previous meanings.

All the above statistical methods were considered in this paper. Perturbation is slight deviation from mean value like SSTA to be $\pm 0.5^{o}C$ from mean value. ENSO is quasi-static periodic. The periodic properties can be represented by Fourier series. All the above statistical technique and its wave nature of signal processing (FFT filters and spectrum analysis) can be done by powerful software (like Matlab, ORIGIN PRO8, data analysis and Graphics design work space, etc.). However the software performs according to concepts of statistical techniques and theory of science. For this work ORIGIN PRO-8 software has been used.

Unit 5

Result and discussion

5.1 Visual judgment

Once missed data were interpolated using trend analysis, a visual judgment has affirmed that the filtered RFA data has clearly exhibited all ENSO events, with some time lag (Fig. 5.1). As it can be seen from the figure, as SSTA increases in the eastern cost of pacific, which is an indication of El Niño, the amount of rainfall in most of the rain gauge stations in Ethiopia decreases. The peaks on most stations such as on Addis Ababa (1964-1968), Jimma (1965-1974), Gambela (1980-1984) are positively correlated. This is not however always true, because mostly it is negatively correlated.

In period from 1998 to 2004 the peaks in the Borena and Mega stations has a positive correlation. During the rest of the time the relation is marked by negative correlation. Previous work (Babu, 1999b) however showed that all are negatively correlated. As it can also be seen from the other stations, the general trend is that, for the south and south eastern part of the area the correlation is in general positive and for the remaining locations it is negative. This observation is also supported by the idea that El Niño will shift positions of ITCZ in such a way that during El Niño event the areas south and south eastern part of the tropical zone has an advantage in such a way that rainfall increases, whereas the remaining locations will have deficiency of rainfall (Babu, 1999; Kassahun, 1999).

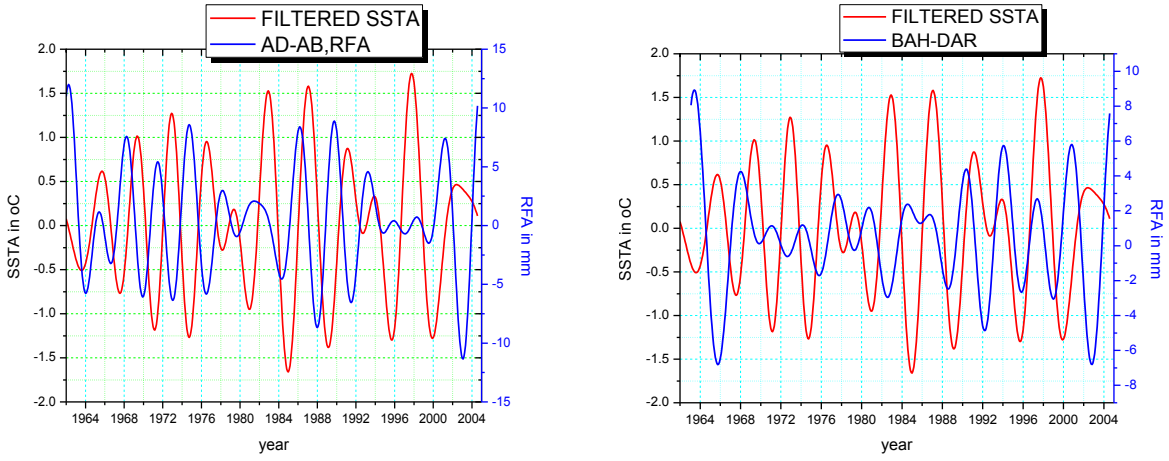

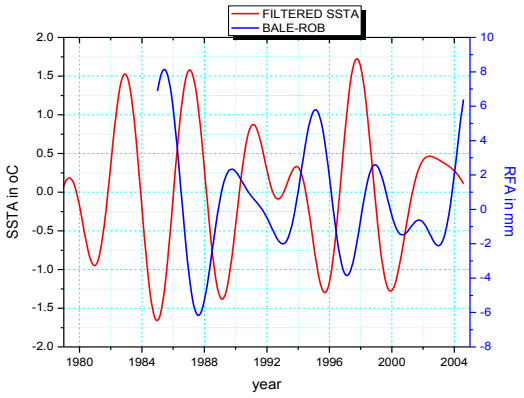
FILTERED SSTA
BALE-ROB
SSTA in oC
RFA in mm
year

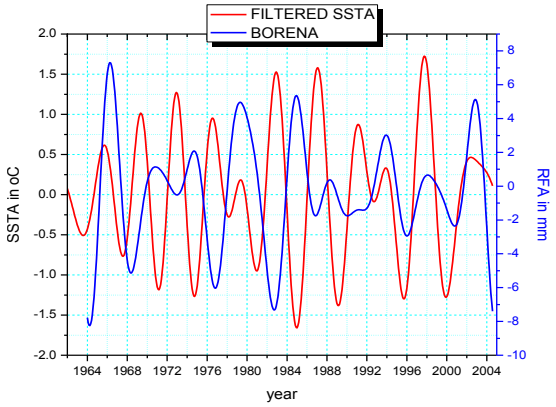
FILTERED SSTA
BORENA
SSTA in oC
RFA in mm
year

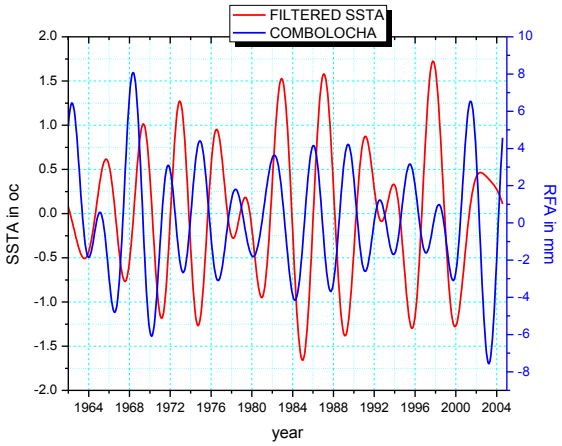
FILTERED SSTA
COMBOLOCHA
SSTA in oc
RFA in mm
year

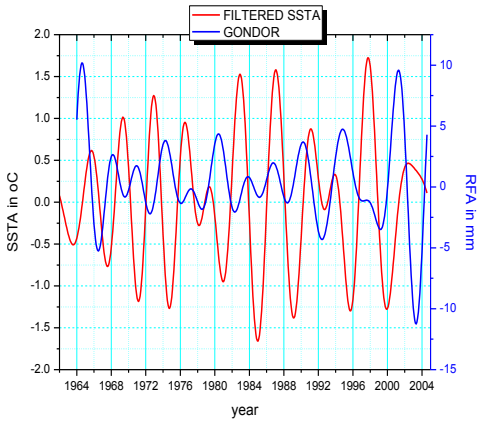
FILTERED SSTA
GONDOR
SSTA in oC
RFA in mm
year

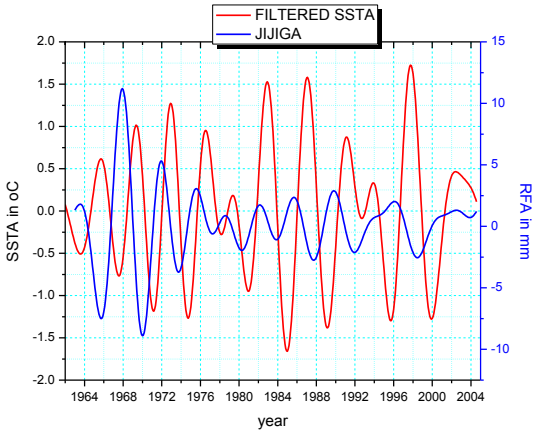
FILTERED SSTA
JIJIGA
SSTA in oC
RFA in mm
year

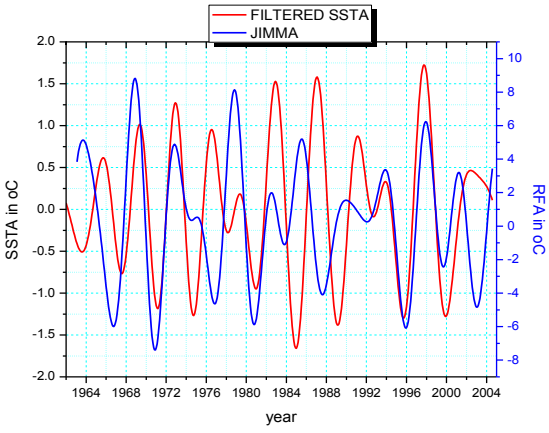
FILTERED SSTA
JIMMA
SSTA in oC
RFA in oC
year

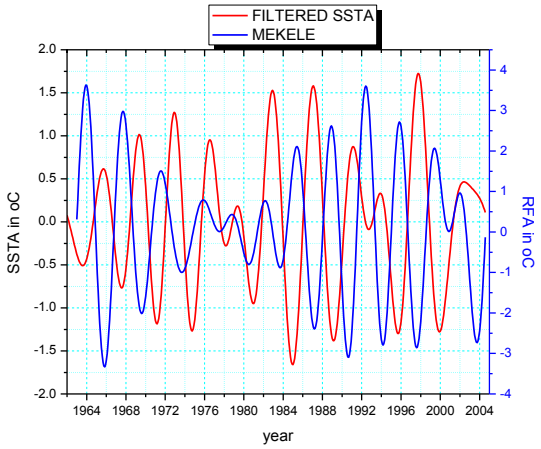
FILTERED SSTA
MEKELE
SSTA in oC
RFA in oC
year

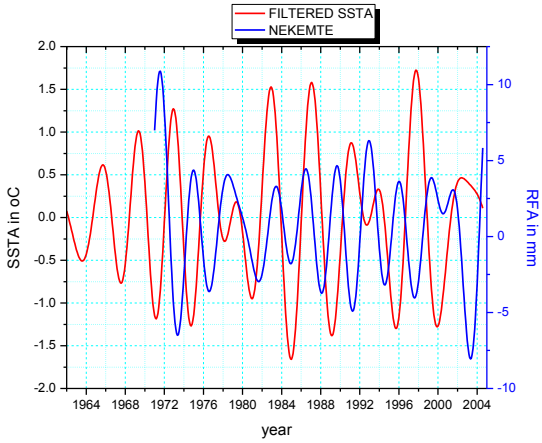
FILTERED SSTA
NEKEMTE
SSTA in oC
RFA in mm
year

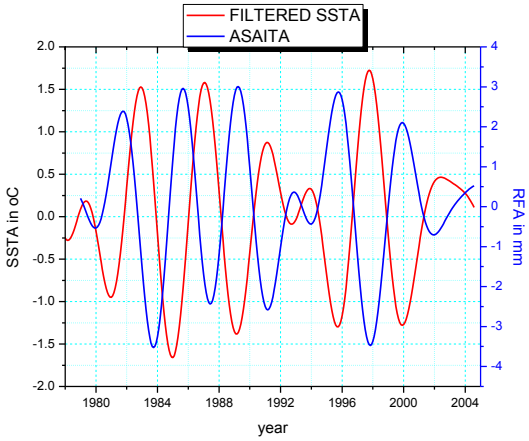
FILTERED SSTA
ASAITA
SSTA in oC
RFA in mm
year

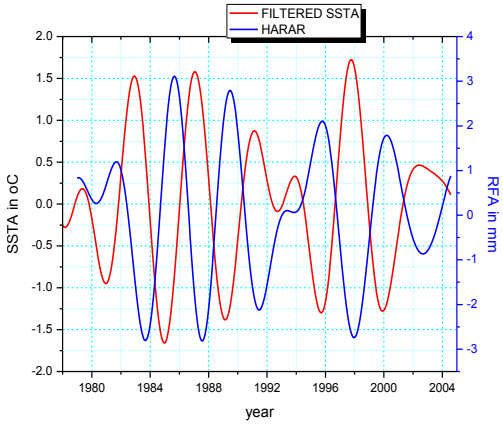
FILTERED SSTA
HARAR
SSTA in oC
RFA in mm
year

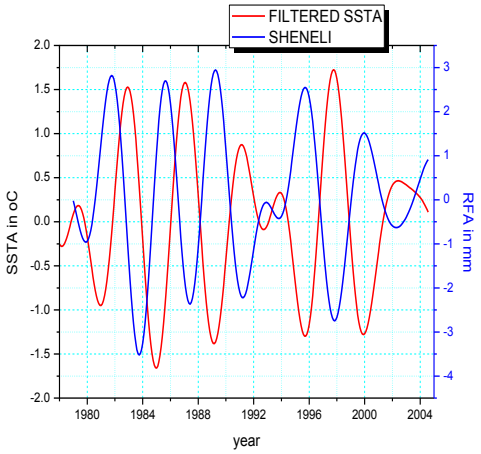
FILTERED SSTA
SHENELI
SSTA in oC
RFA in mm
year

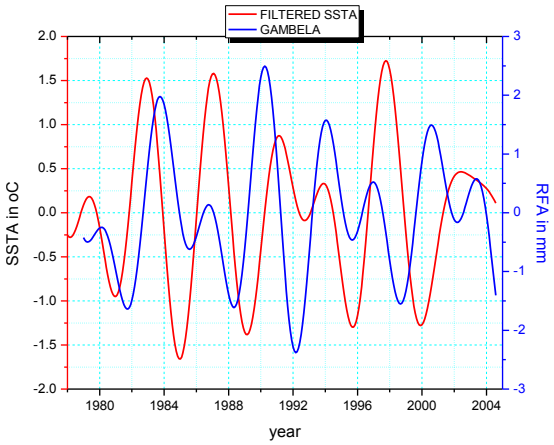
FILTERED SSTA
GAMBELA
SSTA in oC
RFA in mm
year

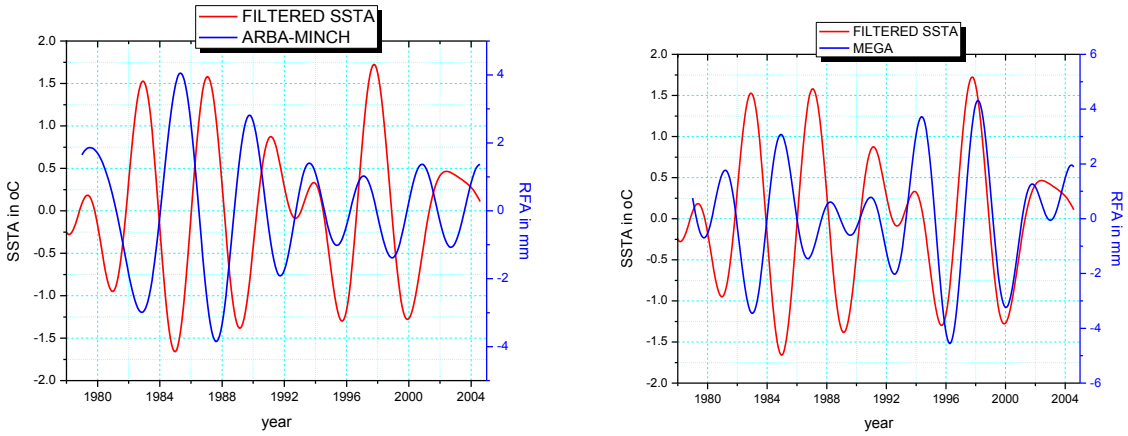

Figure: 5.1: Filtered SSTA with filtered RFA for the different stations throughout Ethiopia.

5.2 Co relational analysis result

After the visual comparison, the next step taken to study the relation between SSTA and RFA was the correlation analysis. The result of this analysis is given in appendix- B. The summary of these plots is presented in Table 5.1. As one can also see from the analysis there is a good correlation between ENSO and rain fall pattern with a delay of RFA to ENSO.

For this work two correlation values, namely the first peak and the maximum peak of the magnitudes of correlation in plots of appendix-B are of interest. The correlation analysis that has been carried out is a cyclic cross-correlation analysis between SSTA and RFA. As one can see from Table 5.1 the first lag correlations of Asaita, Shinile and Harar showed the strongest negative correlation with an average of 0.85, whereas Arba-Minch, Addis Ababa, Mekele, Combolcha and Jijiga have relatively stronger negative correlation with an average of 0.57. The remaining locations have a negative correlation with an average value of 0.3. Though this has agrees well with previous work (Babu, 1999b). Borena, Mega, Robe and Kebri-Dar have positive correlation with an average of 0.22, it has shown that there is a systematic spatial variation in correlation.

These different correlation values are exhibiting the different microclimate zones, which is in good agreement to what has been discussed about the relation between ITCZ and ENSO.

The investigation of the time lag in relation with the correlation analysis showed that RFA in most locations have strong correlation with a delay time of 4 to 5months. On the other hand the second category of negative correlation of 0.57 has a delay time of 6 to 8 months (except Mekele that has a one month delay). The remaining locations that showed negative correlation have time lag between 4 to 12 months.

Low land areas of Kebri-Dar and Mega showed a delay of 9 to 11 months whereas Robe and Borena have almost 21 months delay after ENSO occurrence. In the positive correlation areas, which show that El Niño resulted in abundance of rainfall, has longer a delay relative to the negatively correlated areas.

Table: 5.1 First lag correlation value table of the above graphs

Name of location	Longitude In degree	Latitude In degree	1st lag corr. value	1st lag time(month)	Max. corr. value	Max. corr. Lag(month)
Gambella	34.58	8.25	-0.30	-14.00	-0.52	-63.00
Nekemte	36.55	9.08	-0.33	-2.00	-0.33	-3.00
Jimma	36.83	7.68	-0.25	-15.00	-0.40	-57.00
Arba Minch	37.55	6.08	-0.66	-6.00	0.73	-31.00
Bahir Dar	37.38	11.06	-0.18	-10.00	-0.44	-212.00
Gondor	37.5	12.6	-0.30	-4.00	-0.56	-68.00
Mega	38.25	4	0.20	-9.00	0.59	-135.00
Addis Ababa	38.7	9.033	-0.52	-7.00	-0.52	-8.00
Mekele	39.47	13.5	-0.58	-1.00	-0.58	-1.00
Borena	39.58	5.317	0.23	-21.00	-0.33	-162.00
Combolcha	39.72	11.067	-0.52	-9.00	-0.52	-9.00
Robe/Bale	40	7.133	0.22	-21.00	0.34	-92.00
Asaita	41.43	11.57	-0.82	-4.00	-0.82	-4.00
shinile	42	10.33	-0.80	-5.00	-0.80	-5.00
Harar	42.12	9.32	-0.89	-5.00	-0.89	-5.00
Jijiga	42.79	9.35	-0.55	-8.38	-0.55	-8.38
Kebri Dar	44.17	6.92	0.011	-11.00	-0.46	-75.00

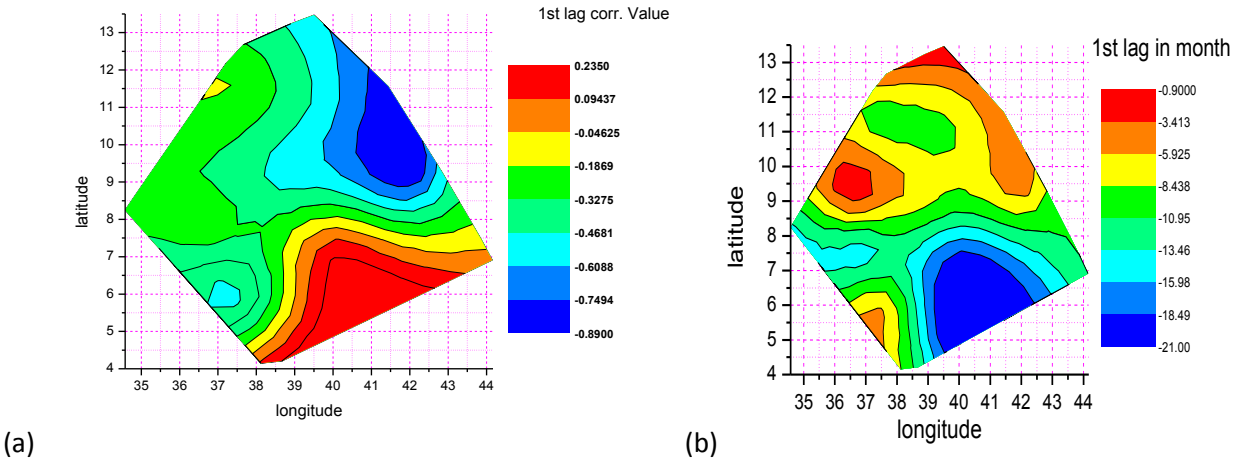

Figure 5.2: Contour graphs of result of Table 4.1

The contour plots given under figure 5.2a shows the spatial distribution of the correlation value, which has a negative correlation around Asaita(Afar), Mekele(Tigray), Shinile(Somali), Combolcha(Wello), and Addis Ababa locations. There is also a negative correlation on south western parts of the country. On the other hand the effects of ENSO observed in south and south eastern parts of the country have a positive correlation with RFA. Since SSTA has weak positive correlation in the south and southeastern part and there are other causes that might have an influence in the same wavelength, further investigation is needed to verify results.

Fig. 5.2(b), show average time lag between SSTA occurrence and peak values of RFA. The effect of SSTA is traced by the RFA with a time lag of 1 to 6 months of North, North eastern and west parts of the country and with a time lag of 8 to 12 months around the central, east and south western parts. In contrary to these locations in the south and south eastern part show 13 to 20 months of time lags. Since their correlation value is also small, further investigation is needed, though the result shows systematic pattern and indicates a natural phenomenon.

5.3 Spectrum analysis result

Another analysis that has been carried out tin this work is the coherency analysis. The aim of this analysis was to identify the frequencies of ENSO that are influencing the rain fall pattern in Ethiopia. The results of the spectrum analysis are given on Table 5.2. But results of the spectrum analysis for the different stations are given in Appendix C.

As one can, for example, see from the power spectrum of SSTA, it has the highest peak at the frequencies 0.281 cycles per year which is a period of 3.55years. This indicates that the period of 3.55 years is the most influential period of ENSO. There are some other local maxima that occurred within the range of 0.187 to 0.328 cycles per year.

The power spectrum analysis of the RFA at the different station also showed that in most stations the influential period is 3.55 years and other local maxima occurred between the 0.187 and 0.328 cycles per year frequency ranges. Here it should be noted that all other effects below the period of 3 years and above 7 years are filtered out. Except some spectral leakage influences outside the aforementioned window are not also expected in the data. The other analysis in the frequency domain is the cross-spectrum analysis. The results of the power and cross spectrum analysis for SSTA and RFA as well as between SSTA and RFA respectively are given in appendix-C. These results are also summarized on Table 5.2.

As it can be seen from column 4 of Table 5.2 the Gambela, Mega, AddisAbaba, Mekele, Combolcha, Asaita and Shinile stations power spectrum has a maximum value around 3.55years. This is also the peak frequency of SSTA. The remaining stations have their maxima in the periods from around 4 to 5 years.

In general all peak values of power spectrum of RFA occurred during the period of 3 to 5 years. Since this period is also the quasi periodic ENSO period and since the cross spectrum analysis also affirmed this fact we can conclude that ENSO affect RFA in the period 3 to 5 years. The effect of the different frequencies is also dependent on the spatial location.

Finally the result of the correlation and coherency analysis are tested for their significance with a tolerance value of 95% and all have shown that the results obtained are significant.

Table 5.2: Shows spectrum analysis of amplitude graph result for each location.

Name of location	(Long., Lati.) In degree	Max. Amp. Frequency occurred for power spectra	Max.Amp. Periods (years) for power spectra	Min amp. Occurred freq.(may have more than two)	Max.Amp. Cross-spectrum period(yrs)
(1)	(2)	(3)	(4)	(5)	(6)
SSTA	(120W,2S)	0.281251	3.5555429	0.328, 0.187	-
Gambella	(34.58,8.25)	0.300001	3.333322222	0.167, 0.233	5.9880
Nekemte	(36.55,9.08)	0.326734	3.060593633	0.149, 0.267	3.7453
Jimma	(36.83,7.68)	0.192386	5.197883422	0.144,0.240	5.2083
Arba Minch	(37.55,6.08)	0.2000008	4.99998	0.267	5.0000
Bahir Dar	(37.38,11.06)	0.1923855	5.197896931	0.120, 0.265	3.4602
Gondor	(37.5,12.6)	0.1967221	5.083312958	0.148, 0.270	5.0761
Mega	(38.25,4)	0.300001	3.333322222	0.233	5.0000
Addis Ababa	(38.7,9.033)	0.32812631	3.04760688	0.2813,0.188	3.7037
Mekele	(39.47,13.5)	0.288001	3.472210166	0.144, 0.240	3.4722
Borena	(39.58,5.317)	0.22131236	4.518500437	0.148, 0.320	4.5249
Combolcha	(39.72,11.067)	0.30468872	3.282038151	0.211	3.5587
Robe/Bale	(40,7.133)	0.20339064	4.916647002	0.102, 0.305	4.9261
Asaita	(41.43,11.57)	0.266668	3.74998125	0.133, 0.200	3.7453
shinile	(42,10.33)	0.266668	3.74998125	0.133, 0.200	3.7453
Harar	(42.12,9.32)	0.200001	4.999975	0.133, 0.267	5.0000
Jijiga	(42.79,9.35)	0.216001	4.629608196	0.144, 0.264	3.4722
Kebri Dar	(44.17,6.92)	0.166667	5.999988	0.300	5.0000

Unit 6: Conclusions

Conclusions

The first part of the study revealed that the amplitude and long term pattern of satellite and rain gauge data were not similar. To solve this problem, it was necessary to develop some strategy to reproduce the rain gauge data from the satellite data. The mathematical approach used for this purpose was the trend analysis between rain gauge data and satellite data. Using this approach it was possible to reproduce rain gauge data from satellite data. The result has been used to fill the gap in the rain gauge data.

The filtering of the RFA and SSTA data was conducted in the frequency domain using Butterworth filter by selectively removing undesired frequencies from the signal. This approach is found to have a great advantage in keeping data with the ENSO‘s period and it was not altering the time lag.

Correlations of filtered SSTA and RFA resulted in negative correlation in most of the stations except on those in the south and south-eastern parts of Ethiopia. Some stations showed very small positive correlation which indicate that they have rainfall abundance during El Niño period. These can also be explained by results from previous work that El Niño forces ITCZ to shift to the south part of its normal location. The different regions of the country are affected by ENSO differently and the time lag between the occurrence of ENSO and RF pattern is also different. Concerning the time lag it is found that RFA lags at an average of 4 to12 months.

Finally spectrum analysis result also showed the detailed relation between ENSO and RFA pattern. All peak values in the power spectrum curve of the RFA indicated that they occur at the peak frequencies of ENSO. Though it is mostly at 3.55 years it in general lies from 3 to 5 year. This also affirmed by the coherency analysis.

In general the outcome of this research work can be used to predict possible occurrence of rainfall shortage in some part of the country and the related drought. In general the drought occurrence in the Northern part of the country (Noted by Welde-Giorgis, 1997) also agrees with strong ENSO quasi-periods of 3 to 5 years. This will lead us to the conclusion that using the information delivered by NOAA-CPC of ENSO phenomena it is possible to predict Ethiopian RF pattern and also the possible occurrence of drought in Ethiopia.

Unit 7: Recommendations

Because of the quasi-periodic nature of the ENSO events, and to affirm the time lag obtained in the time domain analysis, it is recommended to further analysis phase lag in frequency domain.

Agricultural sector

As one can see ENSO phases (Glebushko, 2004), one cannot underestimate the importance of El Niño forecasting for many regions of the world, especially for those countries in tropical regions where economic success is based on fisheries, agriculture and food production, all of which depend on weather patterns. Peru is an excellent example of a country that derives huge economic benefits from El Niño forecasting. Usually a warmer than normal year with moderate and strong El Niño onset is unfavorable for fisheries. When the state of equatorial Pacific is near normal conditions are favorable for agriculture. La Niña conditions (colder than normal ocean surface temperatures) are good for fishing, but not favorable for farmers, bringing them drought and crop failure. El Niño affects the amount of precipitation, so forecasts help to decide when it‘s better to sow rice (in expected wetter periods), and when to sow cotton (in drier periods). Review literature showed this was started in Ethiopia.

Health sector

In a similar manner (Hales et al., 1999; Poveda et al., 2001) has given that ENSO may have an effects of health sector; epidemic disease like malaria from the usual conditions, dengue fever (tropical viral disease by vector born disease like mosquito) and leishmaniasis (a tropical and sub-tropical disease caused by leishmania (single celled protozoan which is transmitted to vertebrates) and transmitted by the bit of sandflies, which is a small hairy biting fly of tropical and sub-tropical regions, which transmits a number of disease). This type of analysis and investigation will also be of importance in the Ethiopian context.

Frequent floods and dam protection

ENSO can affect the discharge rate of flows of rivers (Quinn, 1992); since its quasi-static periodic nature, researcher must be done in each of Ethiopian rivers and lakes discharge rate for the protection of sudden effect. Dam construction and early warning of floods across river should be focused. This will be done if ENSO correlation with discharge rate. Researchers have been done in Egypt about Nile rivers discharge rate during ENSO events.

All the above concepts can be recommended as the possible effects of ENSO on Ethiopian locations. However lack of well documented and quality data may cause the research becomes more difficult and low reliability of the work.

References

[1]Abate, Kefialew, 1984. Trends and variation of some climate elements at three stations in Addis Abeba, MA thesis, Dept. of Geography, Addis Ababa University.

[2] Babu, A (1999a), (NMSA). Lecture Notes: The Main Synoptic Features Affecting Ethiopia During the Different Seasons. National Meteorological Services. 1st DMC Nairobi Capacity Building Workshop, 11 January to 15 February 1999. Unpublished Lecture Notes.

[3]Babu, A (1999b). (NMSA). Lecture Notes: The Impact of Pacific Sea SurfaceTemperature on the Ethiopian Rainfall. 1st DMC Nairobi Capacity Building Workshop,11 January to 15 February 1999. Unpublished Lecture Notes.(coated by T. W. Giorgis,The Case of Ethiopia, July 2000)

[4] Bekele, F., 1993: Probability of Drought Occurrence under Different Events, NMSA. Addis Ababa, Ethiopia.

[5] Bekele, F. 1997. Ethiopian Use of ENSO Information in Its Seasonal Forecasts, Internet Journal of African Studies. No. 2. March. http://www.brad.ac.uk/research/ijas/ijasno2/ijasno2.html

[6] Bjerknes, J., 1966: A possible response of the atmospheric Hadley circulation to equatorial anomalies of ocean temperature. Tellus, 18, 820-829

[7] Boer, G.J. and Yu, 2002: Climate sensitivity and response. Springer-Verlag 2002, Climate Dynamics (2003) 20: 415–429

[8] Cane, M.A., S.X. Dolan, and S.E. Zebiak, Experimental forecasts of El Niño, Nature, 321, 827-832, 1986.

[9] Brillinger, D. R., 1975, Time series: Data Analysis and Theory, Holt, Rinehart and Winston, Inc. New York, U.S.A.

[10] Conway, G., Feb. 2008 : The Science of Climate Change in Africa: Impacts and Adaptation,

[11] CPC, 2004(reference year), cold and warm episodes by season, http://www.cpc.ncep.noaa.gov/products/analysis_monitoring/ensostuff/ensoyears.html, home page of the National Oceanic and Atmospheric Administration, National Weather Service, Climate Prediction Center, U.S.A.

[12] Degefu, Workineh. 1987. _Some aspects of meteorological drought in Ethiopia.‘ In Michael H.Glantz (Ed), Drought and Hunger in Africa. Cambridge: Cambridge University Press.

[13] Dinku, T., et al, 2007: Validation of satellite rainfall products over East Africa's complex topography, International Journal of Remote Sensing, 28:7, 1503-1526.

[14] FAO/GIEWS Special Report on Ethiopia. FAO/WFP Crop and Food Supply Assessment Mission to Ethiopia. 19 December 1997.

[15] Glantz, M.H.1996. Currents of Change: El Niño‘s Impact on Climate and Society. Cambridge: Cambridge University Press.

[16] Glebushko, K. (2004) The El Niño phenomenon. From understanding to predicting.CSA 2004 http://www.csa.com/discoveryguides/discoveryguides-main.php

[17] Gonfa, L., 1996: Climate Classifications of Ethiopia. Meteorological Research Reports Series, No.3, May. Addis Ababa, Ethiopia, National Meteorological Services Agency.

[18] Haile, T., 1986. Climate Variability and Surface Feedback Mechanism in Relation to the Sahelo Ethiopian Droughts. Dissertation submitted in partial fulfillment of M.S. degree in Meteorology, Department of Meteorology, University of Reading, Reading, UK.

[19] Haile, T., 1988: Causes and characteristics of drought in Ethiopia. Ethiopian Journal of Agricultural Science, 10, 85-97.

[20] Hales et al., 19 99, El Nino and the Dynamics of Vector borne Disease Transmission Environmental health perspective vol.107 no. 2, February 19 99.

[21] Hortol, R., J, 2004: An introduction to meteorological dynamics, 4th ed., Elsevier Inc. USA

[22] IPCC. (2001a). Climate change 2001: The scientific basis.Cambridge University Press, Cambridge,UK.

[23] IPCC. (2001b). Climate Change 2001: Impacts, Adaptation and Vulnerability. Cambridge University Press, Cambridge, UK.

[24] IRI, Theory of waves. Columbia university http://iri.columbia.edu/climate/ENSO/theory/waves.html

[25] Jackson, I. J. 1979. Climate, Water and Agriculture in the Tropics. London and New York: Longman Groups Ltd.

[26] Jaochin. G. (2008) International Journal for rural development Rural 21 volume 43. The ultra-poor neglected resource, future potential. No.5/2008ISSN: 1866-8011.D20506F

http:// www.rural21.com

[27] Jenkins, G.M., Watts, D.G.:1968, spectral analysis and its application, Holden-Days, San Francisco, U.S.A.

[28] Kassahun, Bokretsion. 1999. Ye'ayer Mezabat'na tinbi'ya k'Itiopia Antsar (Climate Change and Forecast in Ethiopia, in Amharic). Paper Presented at a Meeting organized by the DPPC on Nehase 1991 (Ethiopian Calendar), titled Ye'ayer Mezabat, Dirk'na ye'adega mekelakel b'Itiopia. A discussion organized by the DPPC on Climate Change, Drought and Disaster Prevention in Ethiopia, Addis Ababa, Ethiopia, August 1999.

[29] Kiladas,G.N. and Diaz,H.F. 1989. _Global Climatic anomalies associated with extremes in the Southern Oscillation', J.of Climate,2: 1069-1090.

[30] Lewi,E., and Groten, 2005. Spatial variation of time lag between SSTA and LOD, AVN, No 5, pp 163-169

[31] Mahdi Osman and P. Sauerborn (2000): land and water resources managements in Ethiopia : What did we learn, where do we go? In Universitat Hohenheim (ed), International Agricultural Research: a Contribution to Crisis Prevention, Proc.Int.Agri.Res. Hohenheim, 11-12 october 2000, 138-139.
http://ww2010.atmos.uiuc.edu/(Gh)/guides/mtr/eln/home.rxml

[32] McCarthy, D. D., Petit, G.:2004, IERS Convention, IERS Technical Note No.32,Verlag des BKG, Frankfurt am Main, Germany.

[33] McPhaden, M. J. et al., J. Geophys. Res. 103, 14,169 (1998).

[34] Mitchell, Todd P., John M. Wallace, 1992: The Annual Cycle in Equatorial Convection and Sea Surface Temperature. J. Climate, 5, 1140–1156.

[35] Neelin, J. D. et al., J. Geophys. Res. 103, 14,261 (1998).

[36] Neelin, J. D. and Latif, Mojib: El Niño dynamics. Physics Today, December 1998, 32-36.

[37] Nicholls, N. and R. W., Katz, 1991: Teleconnections and their implications for long-range forecasts. In: Teleconnections Linking Worldwide Climate Anomalies (ed. M.H. Glantz, R. W. Katz & N. Nichollos). Cambridge University press, New York, pp.511-525.

[38] Nicholls, N., 1993: _What are the potential contributions of El Niño - Southern Oscillation Research to Early Warning of Potential Acute Food-deficit Situations?‘ in M. H. Glantz (Ed.), Workshop on Usable Science: Food Security, Early Warning and El Niño, 25 28October, Budapest, Hungary, Boulder: National Center for Atmospheric Research, 169-177.

[39] NMSA (National Metrological Services Agency), (1996): Climatic & Agro climatic Resources of Ethiopia. Meteorological Research Report Series, 1:1, January. Addis Ababa, Ethiopia.

[40] NMSA, 1989. Beginbot 9, sleweqt yekremt azmamya yetesetew tinbit yezet (in Amharic).

[41] NMSA,1998. Annual Climate Bulletin. Addis Ababa, Ethiopia.

[42] NMSA. (2004). Climate of Ethiopia Series. Vol. I, No. 1: Rainfall. Federal Democratic Republic of Ethiopia Ministry of Water Resources. National Meteorological Services Agency. A.Ababa , Ethiopia . P.1-134.

[43] NOAA Webpage: http://www.cpc.noaa.gov/index.php National Weather Services, Climate Prediction Center

[44] Otens, R.K., Enochson, L., 1972, Digital time Series analysis, John Wiley & Sons Inc., New York, U.S.A.

[45] Peixoto, J. P. und Oort, A. H.: Physics of climate. New York, American Institute of Physics, 1992, 173, 415,423, 426, 430.

[46] Picaut et al., Mechanism of the Zonal Displacements of the Pacific Warm Pool: Implications for ENSO.1996, 274 (5292): 1486-1489

[47] Poveda et al. 2001, Coupling between Annual and ENSO Timescales in the Malaria–Climate Association in Colombia. Environmental health perspective vol. 109 no. 5 may 2001

[49] Quinn, W. H. and V. T. Neal, 1987: _El Niño Occurrences Over the Past Four and Half Centuries.‘ Journal of Physical Research, 92:C13, December 15, 14,449-14,461.

[50] Quinn, William. 1992. The Study of Southern Oscillation-related Climate activity from AD 622-1900 incorporating Nile River flood data. In Editors Henry F. Diaz and Vera Markgrat. El Niño, Historical and Paleoclimatic Aspects of the Southern Oscillation. Cambridge: Cambridge University Press. Pages 119-49.

[51] Sirvatka, P., ENSO Notes. IRI, Columbia University.

[52] Storch, H.,V. and Zwiers, F.,W, 19 99: Statistical analysis in climate research. Cambridge university press.

[53] Thompson, R.OR.Y., 1979, Coherence significance levels; Notes and correspondence, Journal of atmospheric Sciences, Vol. 36, 2020-2021.

[54] Trenberth et al. 2002,the evolution of ENSO and global atmospheric temperatures. Journal of geophysical research 107,D8 10.1029/2000JD 000298

[55] Walker, G.T., 1928: World Weather. Monthly Weather Review, 56, 167-170

[56] Welch, P.D. 1967, "The use of Fast Fourier Transform For the Estimation of Power Spectra: A method Based on Time Averaging Over Short , Modified Periodograms."IEEE Trans. Audio Electroacoust. Vol. AU-15, 70-73.

[57] Wilks, D, S., 2006, Stastical methods in the atmospheric science, Elsevier Inc. USA

[58] Wolde-Georgis, Tsegay. 1997. "El Niño and Drought Early Warning in Ethiopia.' In Using Science Against Famine: Food Security, Famine Early Warning and El Niño, Internet Journal for African Studies, Issue No. 2 – April 1997, Michael H. Glantz, special Volume Editor. (http://www.brad.ac.uk/research/ijas/ijasno2/ijasno2.html).

[59] Wyrtki, Klaus, 1979: The Response of Sea Surface Topography to the 1976 El Niño. J. Phys. Oceanogr., 9, 1223–1231

[60] Xie et al. 2003, GPCP Pentad Precipitation Analyses: An Experimental Dataset Based on Gauge Observations and Satellite Estimates, journal of climate vol. 16

[61] Xie, S.-P., 2004: Tropical Atlantic Variability: Patterns, Mechanisms, and Impacts, J. American Geophysical Union Geographical Monograph.

Appendix: A (Trend analysis)

Some of the data interpolated from satellite by selecting best values of R^2 for each location.

(x-satellite and y-rain gauge data in mm)

Nekemte

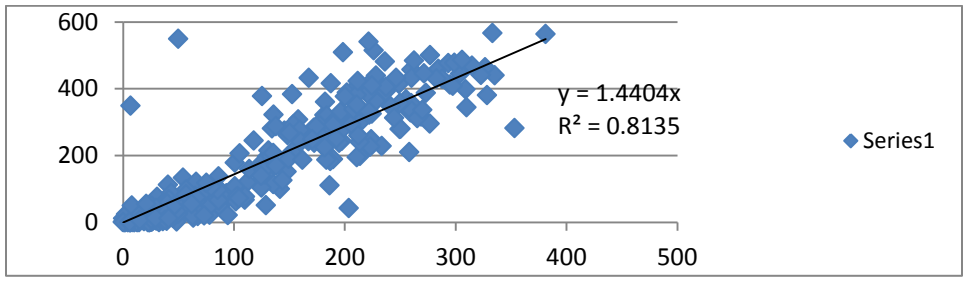

Negele Borena

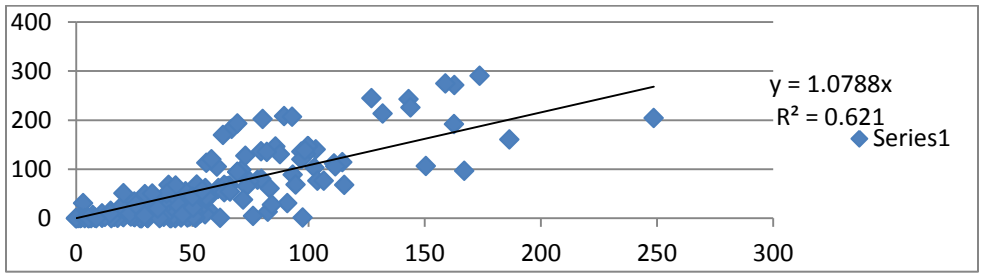

Jimma

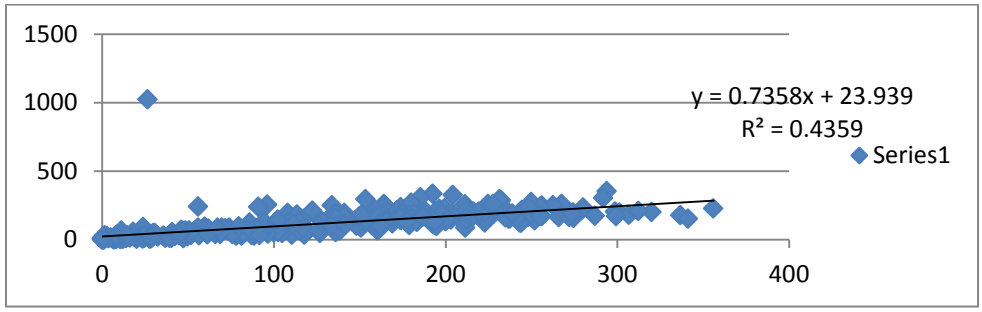

Bahi-Dar

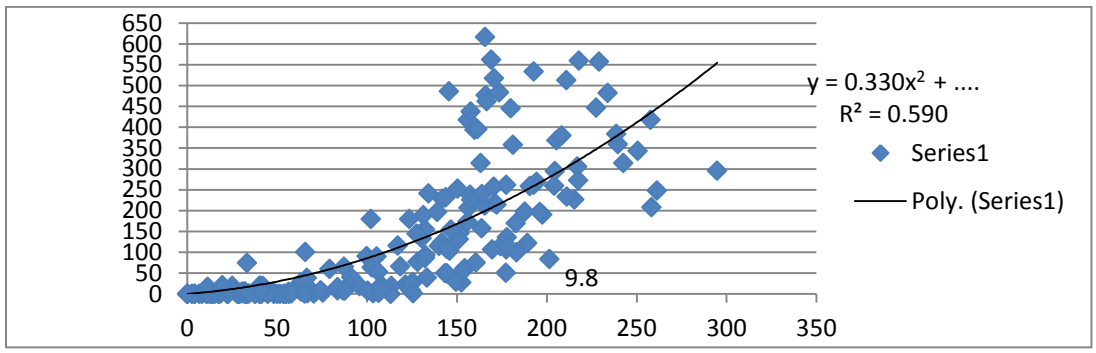

Mekele

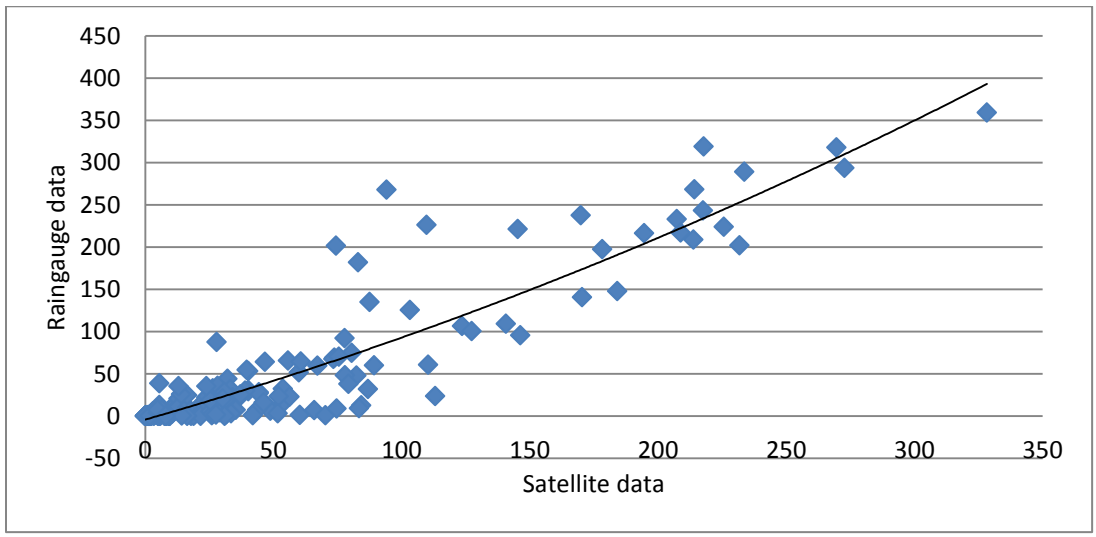

Jijiga

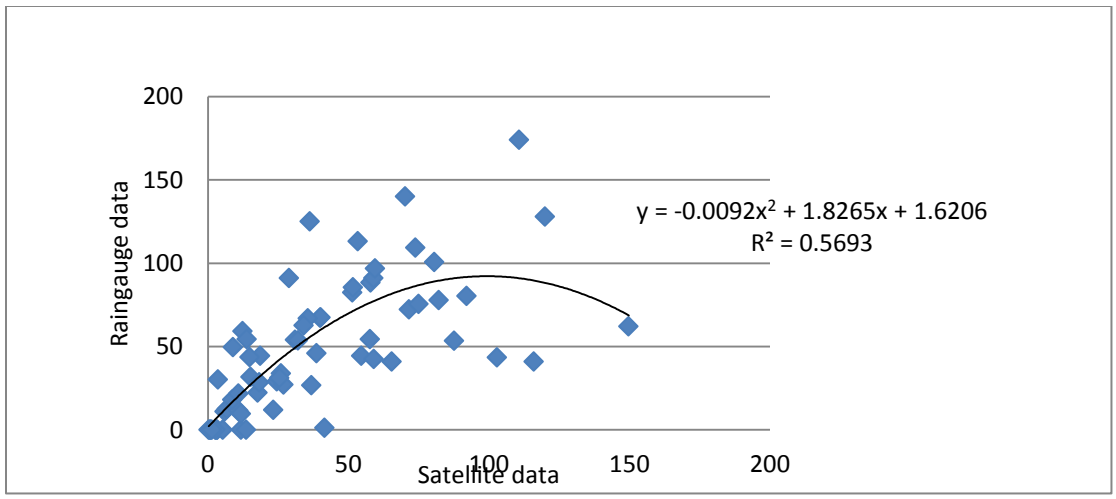

Gondor

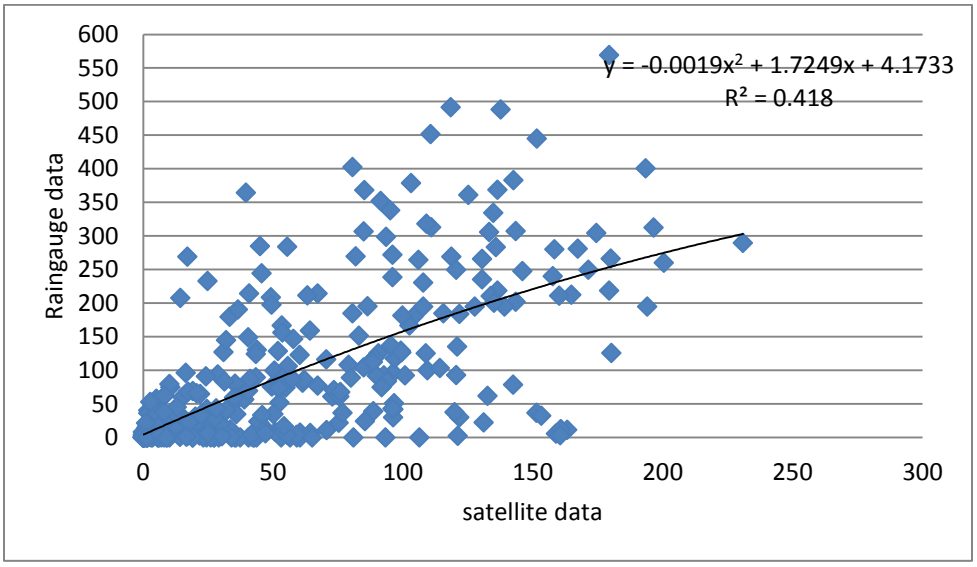

Combolcha

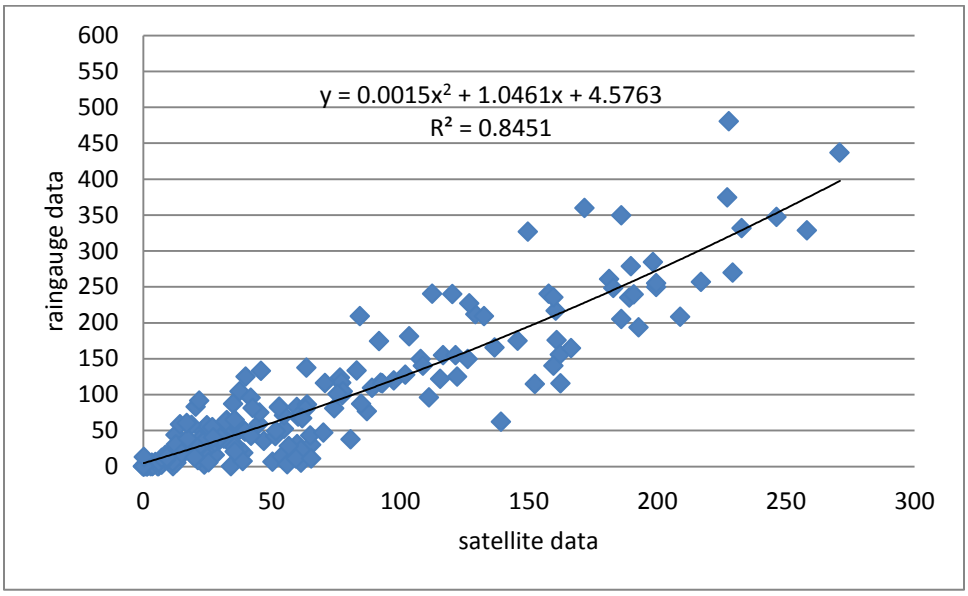

Appendix: B (Cross-correlation graphs, x-as lag in year and y-as correlation value)

Addis Abeba.

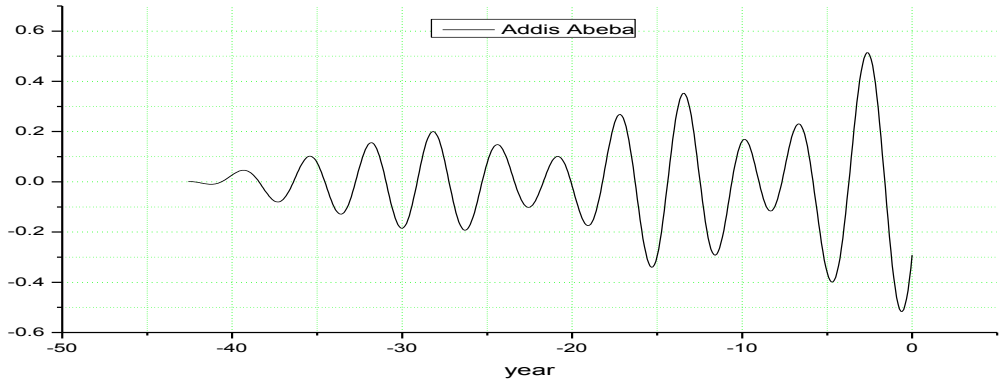

Bahir-Dar

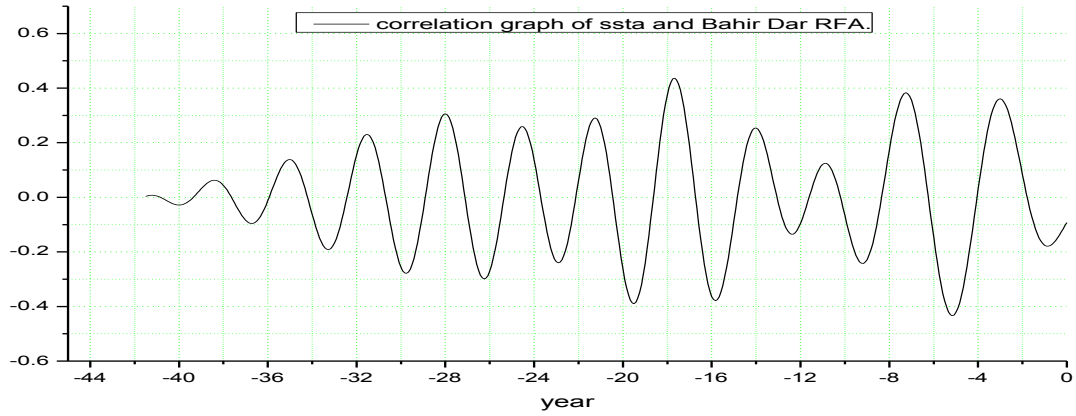

Bale Robe

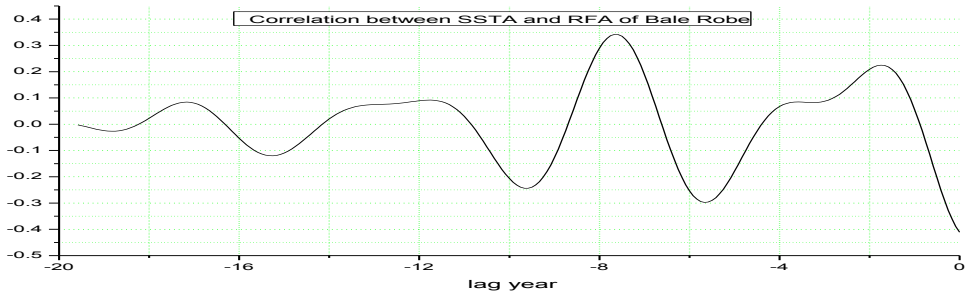

Borena/Negele

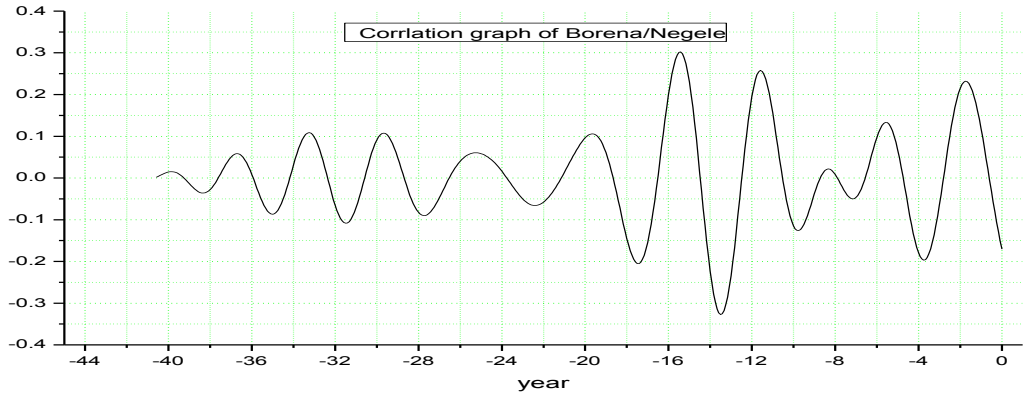

Combolcha

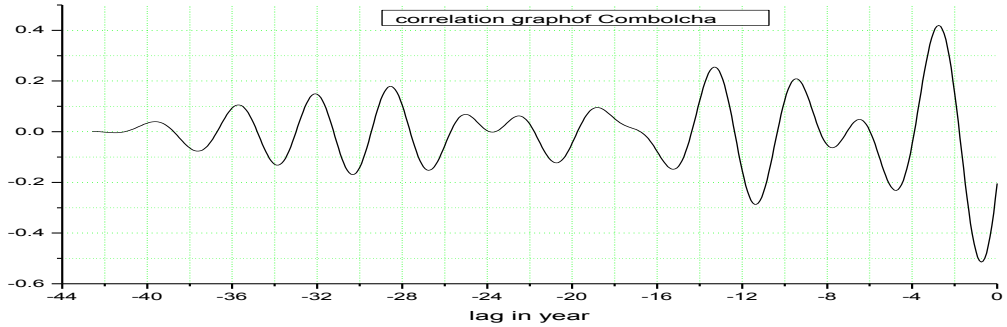

Gondor

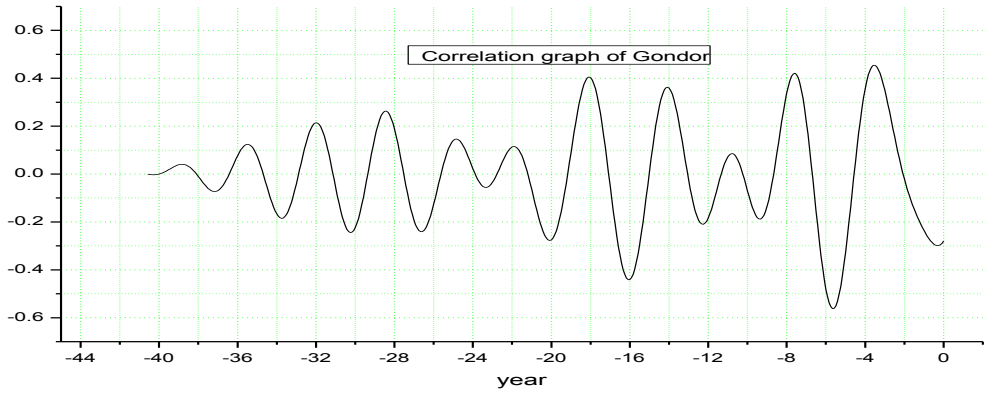

Jijiga

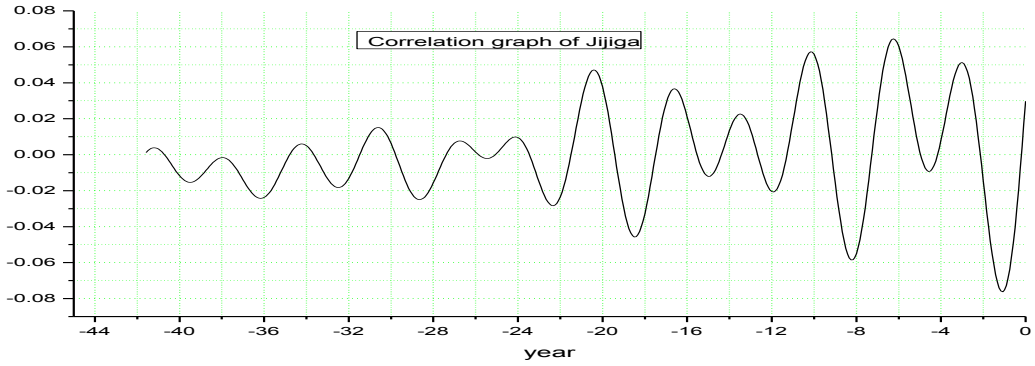

Jimma

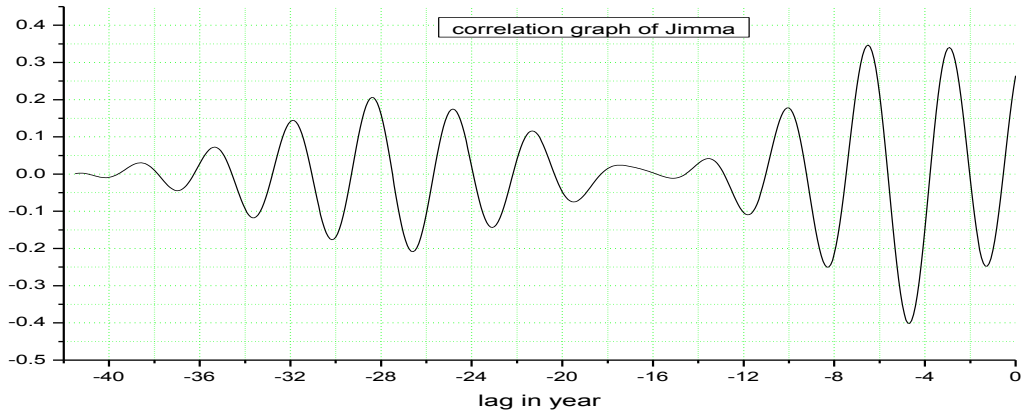

Mekele

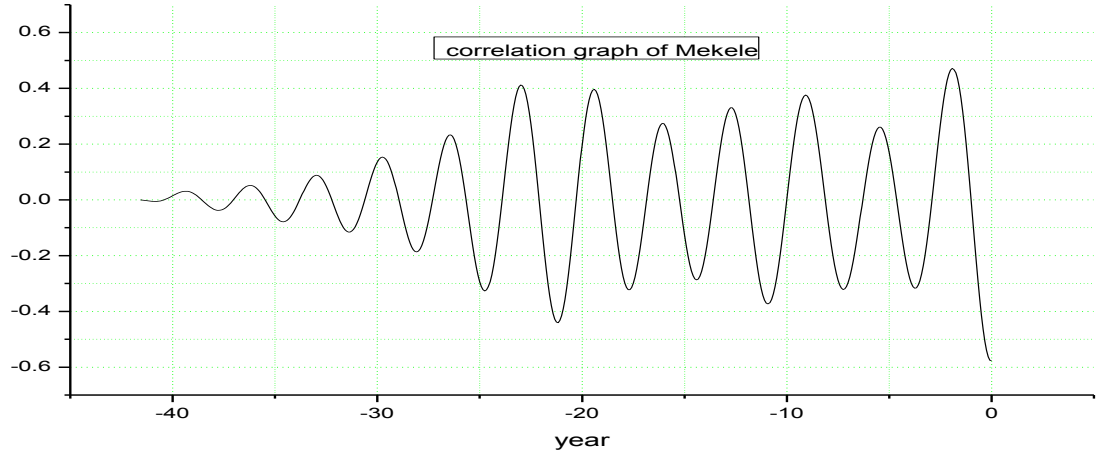

Nekemte

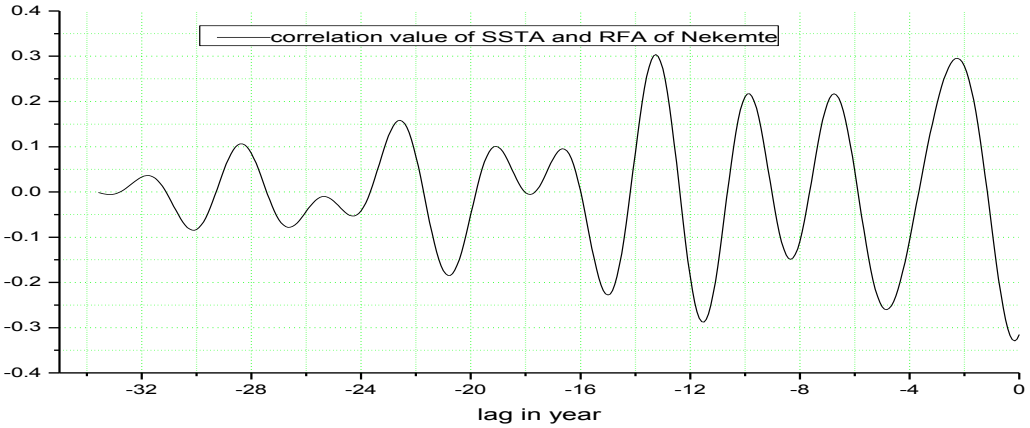

Arba Minch

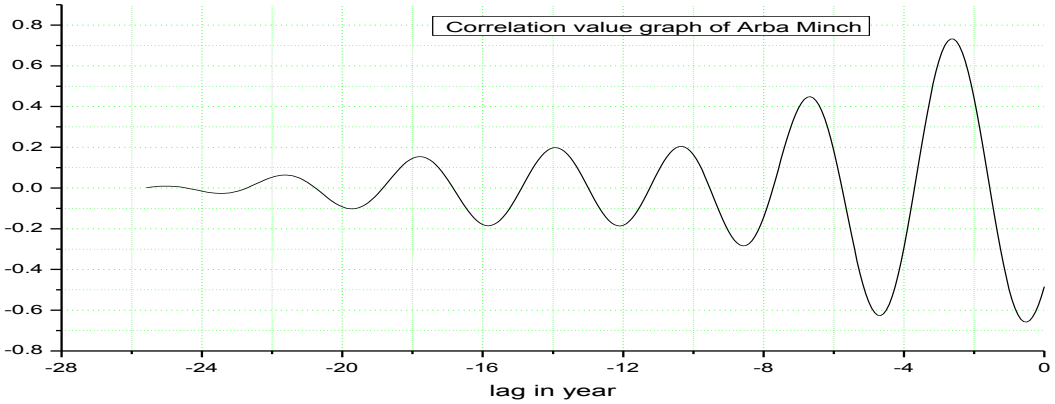

Asaita

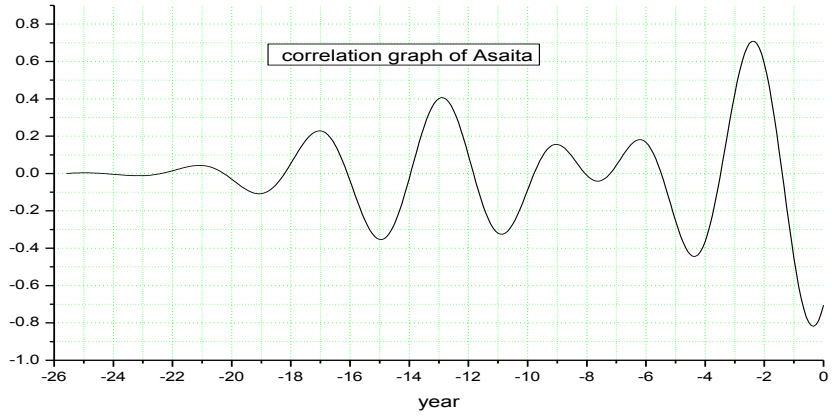

Hara

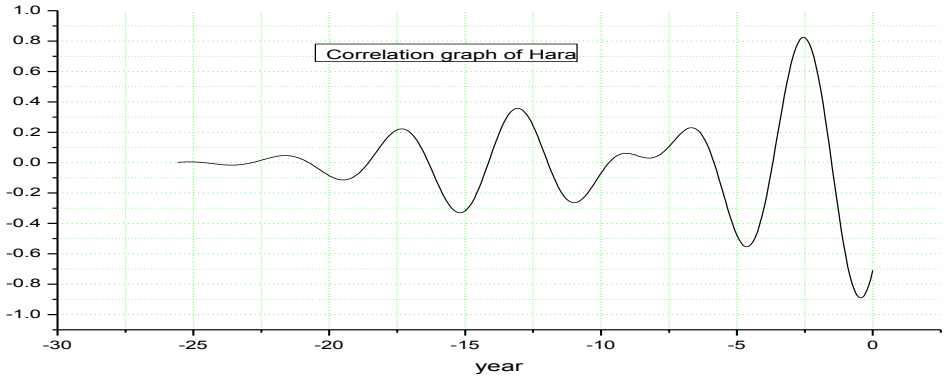

Kebri-Dar (Somali)

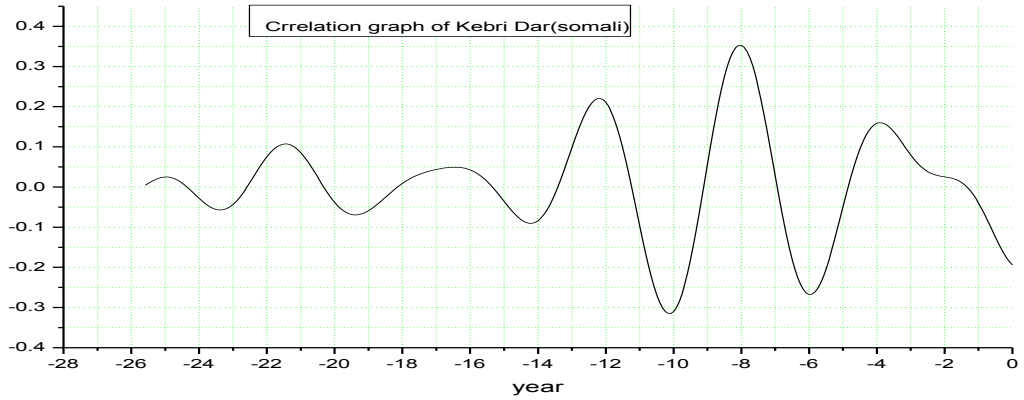

Mega (Southern part of Ethiopia)

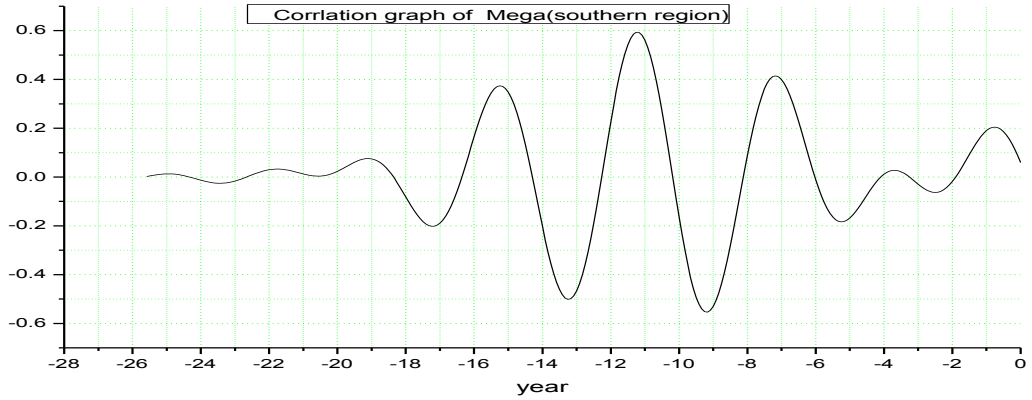

Gambela

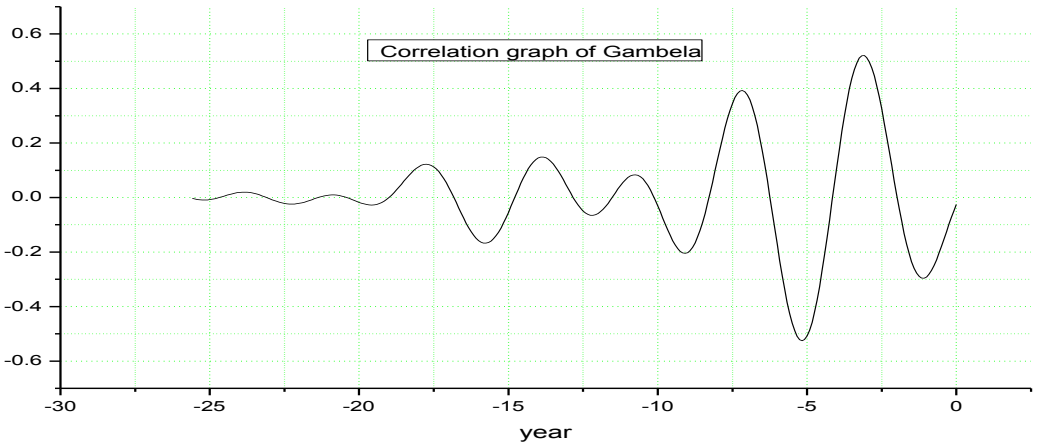

Appendix: C Cross-spectrum analysis, amplitude graph

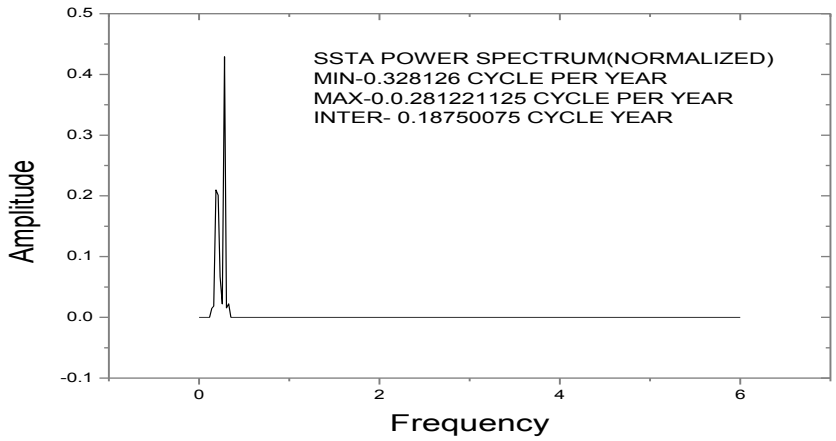

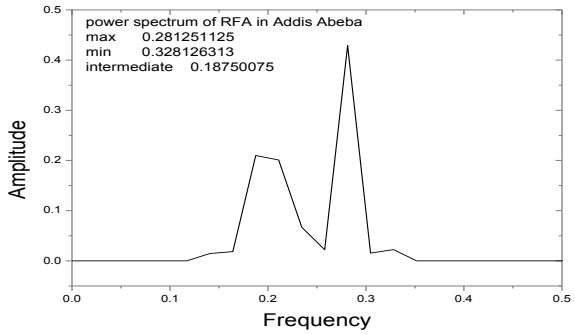

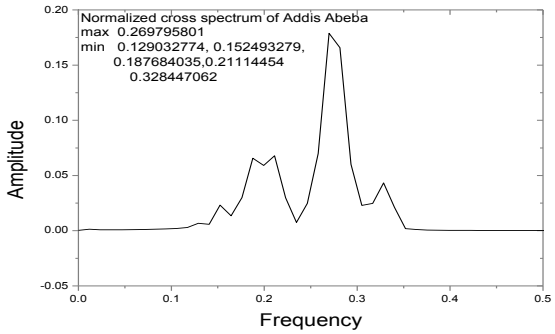

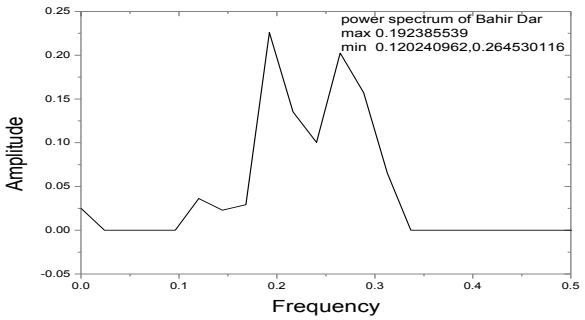
power spectrum of Bahir Dar
max 0.192385539
min 0.120240962,0.264530116
Amplitude
Frequency

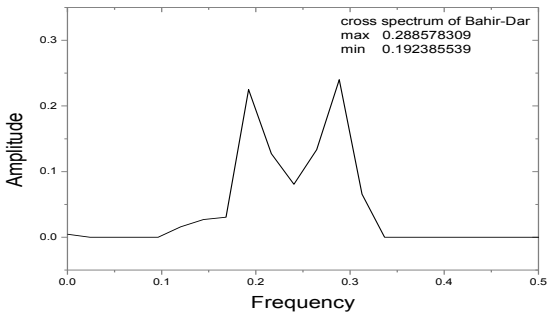
cross spectrum of Bahir-Dar
max 0.288578309
min 0.192385539
Amplitude
Frequency

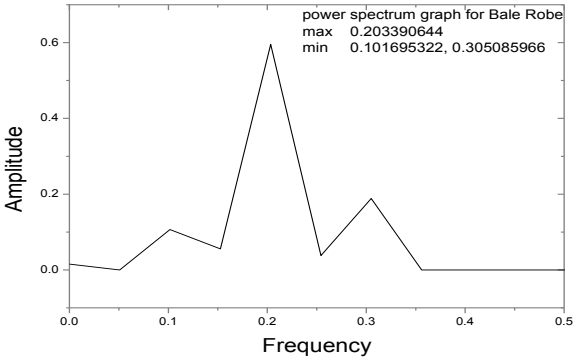
power spectrum graph for Bale Robe
max 0.203390644
min 0.101695322, 0.305085966
Amplitude
Frequency

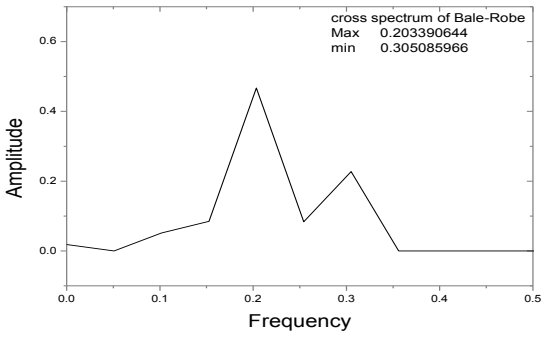
cross spectrum of Bale-Robe
Max 0.203390644
min 0.305085966
Amplitude
Frequency

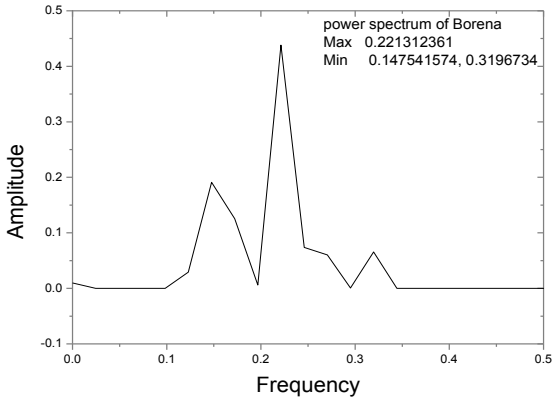
power spectrum of Borena
Max 0.221312361
Min 0.147541574, 0.3196734
Amplitude
Frequency

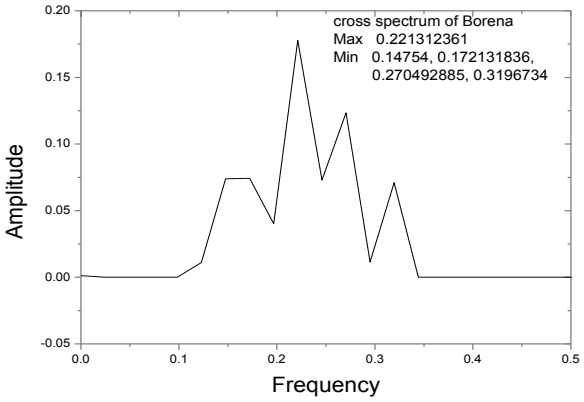
cross spectrum of Borena
Max 0.221312361
Min 0.14754, 0.172131836,
0.270492885, 0.3196734
Amplitude
Frequency

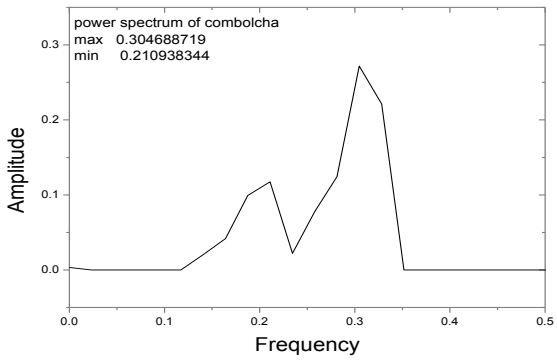
power spectrum of combolcha
max 0.304688719
min 0.210938344
Amplitude
Frequency

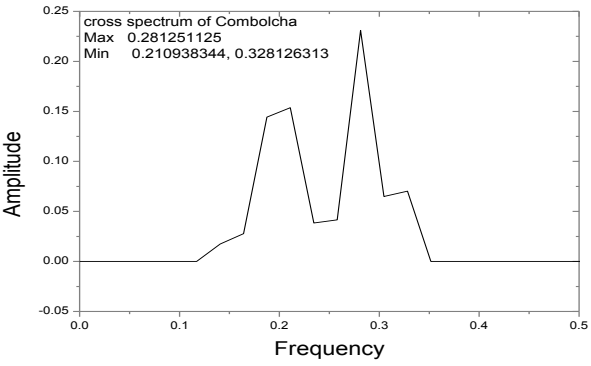
cross spectrum of Combolcha
Max 0.281251125
Min 0.210938344, 0.328126313
Amplitude
Frequency

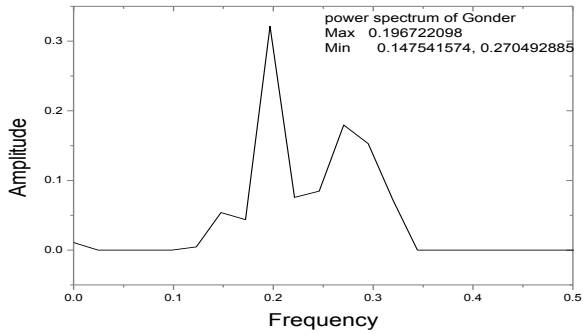
power spectrum of Gonder
Max 0.196722098
Min 0.147541574, 0.270492885
Amplitude
Frequency

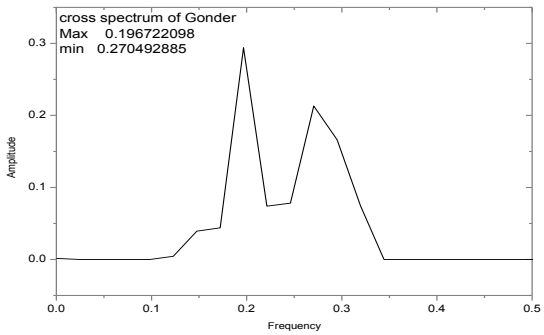
cross spectrum of Gonder
Max 0.196722098
min 0.270492885
Amplitude
Frequency

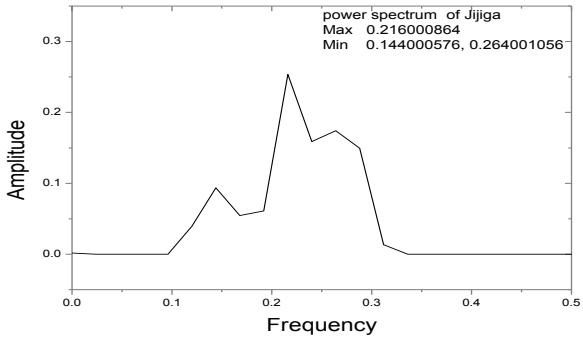
power spectrum of Jijiga
Max 0.216000864
Min 0.144000576, 0.264001056
Amplitude
Frequency

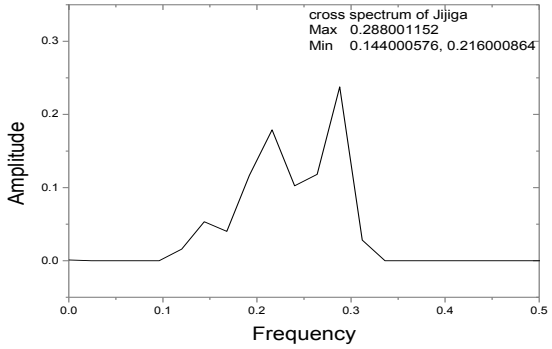
cross spectrum of Jijiga
Max 0.288001152
Min 0.144000576, 0.216000864
Amplitude
Frequency

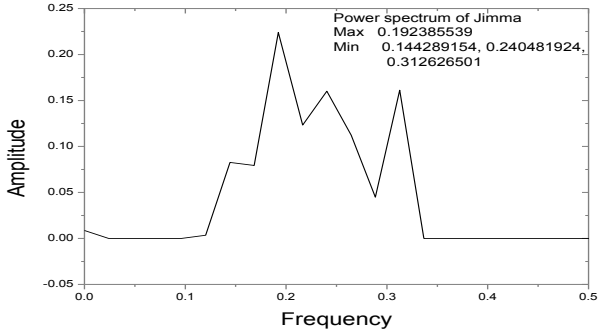
Power spectrum of Jimma
Max 0.192385539
Min 0.144289154, 0.240481924, 0.312626501
Amplitude
Frequency

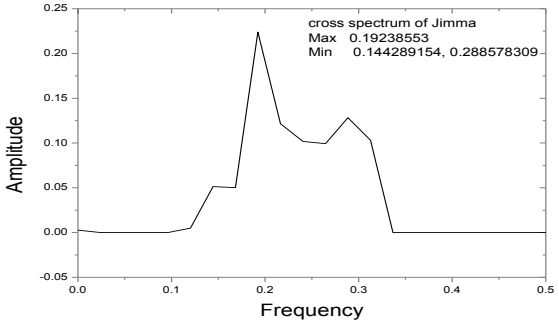
cross spectrum of Jimma
Max 0.19238553
Min 0.144289154, 0.288578309
Amplitude
Frequency

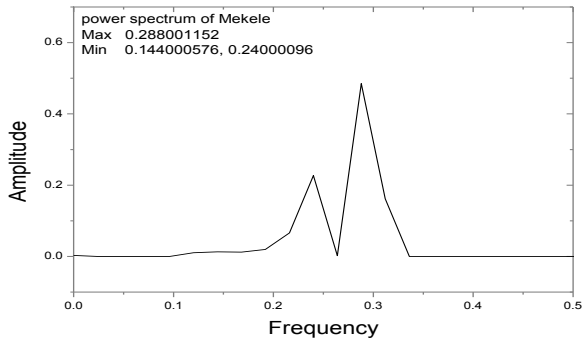
power spectrum of Mekele
Max 0.288001152
Min 0.144000576, 0.24000096
Amplitude
Frequency

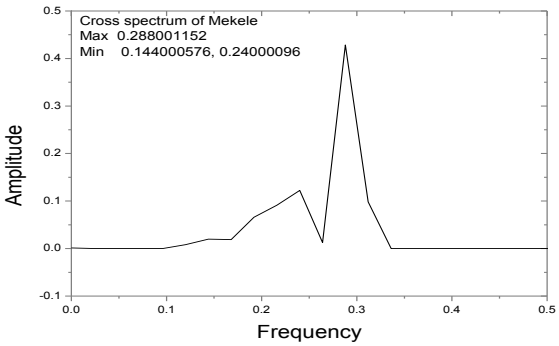
Cross spectrum of Mekele
Max 0.288001152
Min 0.144000576, 0.24000096
Amplitude
Frequency

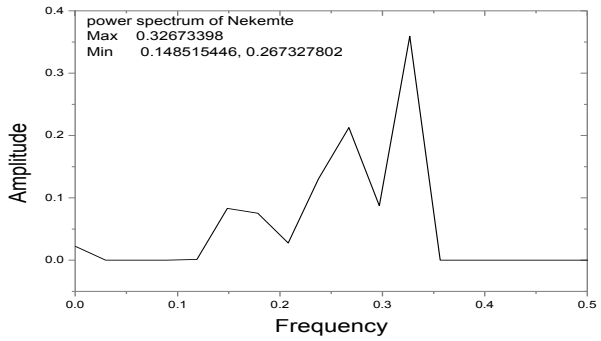
power spectrum of Nekemte
Max 0.32673398
Min 0.148515446, 0.267327802
Amplitude
Frequency

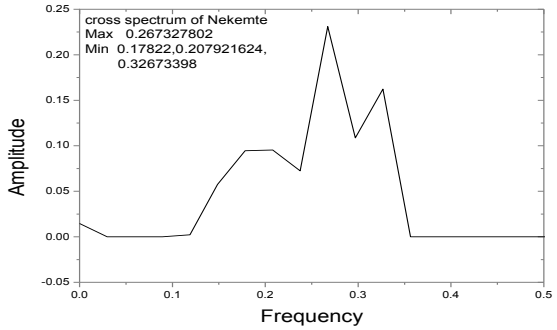
cross spectrum of Nekemte
Max 0.267327802
Min 0.17822,0.207921624,
0.32673398
Amplitude
Frequency

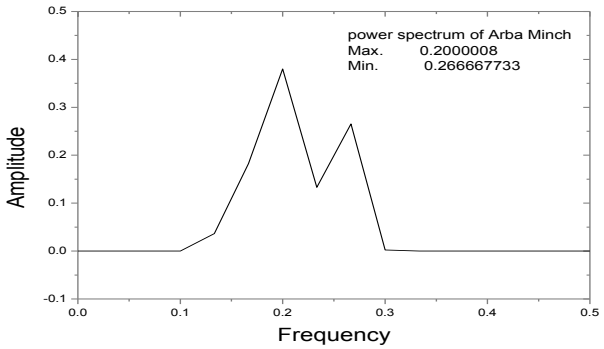
power spectrum of Arba Minch
Max. 0.2000008
Min. 0.266667733
Amplitude
Frequency

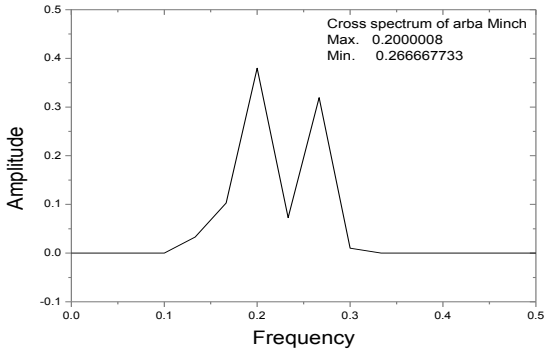
Cross spectrum of arba Minch
Max. 0.2000008
Min. 0.266667733
Amplitude
Frequency

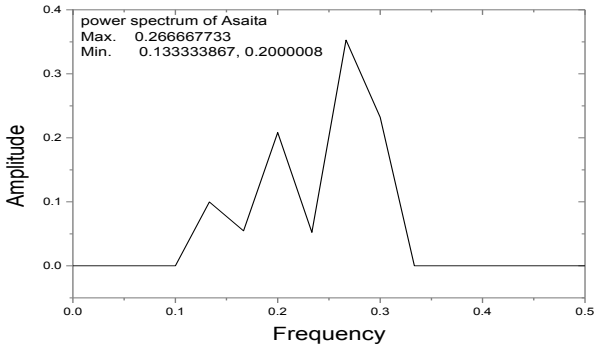
power spectrum of Asaita
Max. 0.266667733
Min. 0.133333867, 0.2000008
Amplitude
Frequency

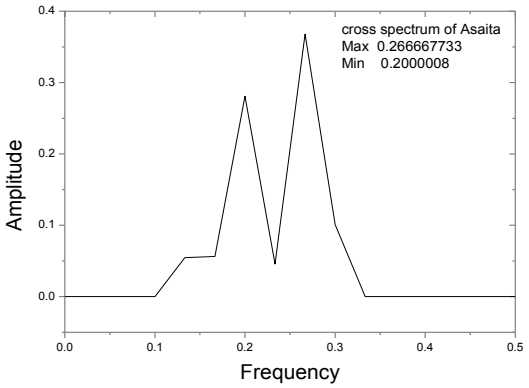
cross spectrum of Asaita
Max 0.266667733
Min 0.2000008
Amplitude
Frequency

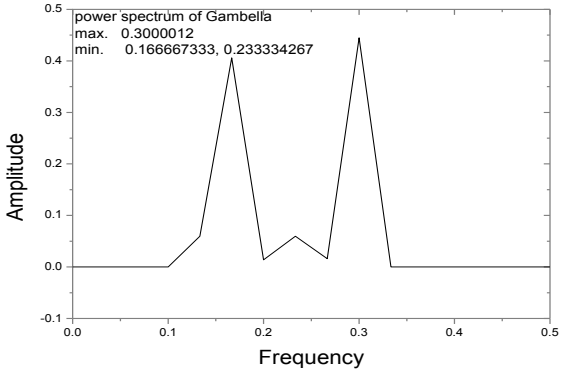
power spectrum of Gambella
max. 0.3000012
min. 0.166667333, 0.233334267
Amplitude
Frequency

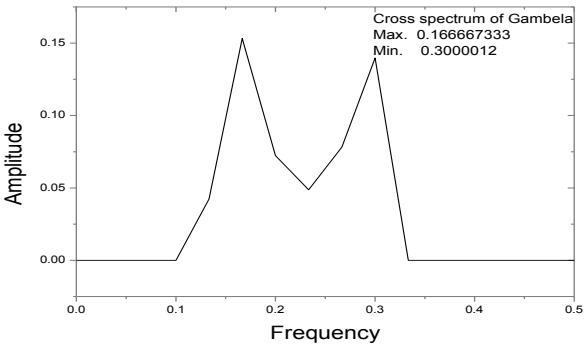
Cross spectrum of Gambela
Max. 0.166667333
Min. 0.3000012
Amplitude
Frequency

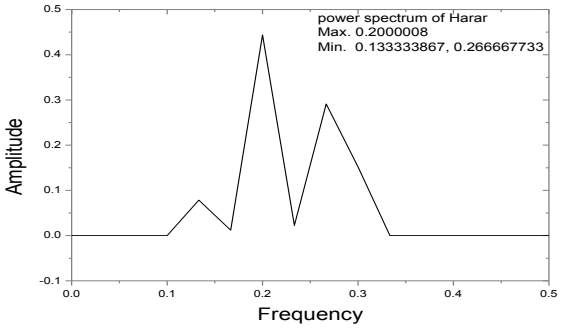
power spectrum of Harar
Max. 0.2000008
Min. 0.133333867, 0.266667733
Amplitude
Frequency

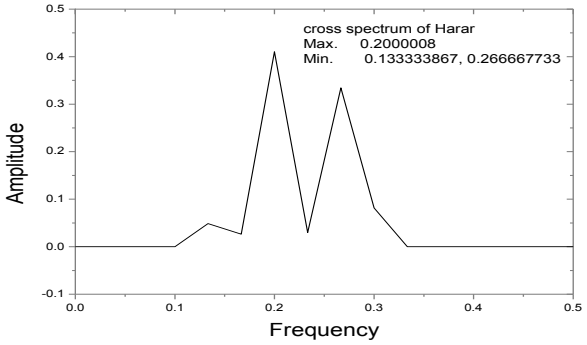
cross spectrum of Harar
Max. 0.2000008
Min. 0.133333867, 0.266667733
Amplitude
Frequency

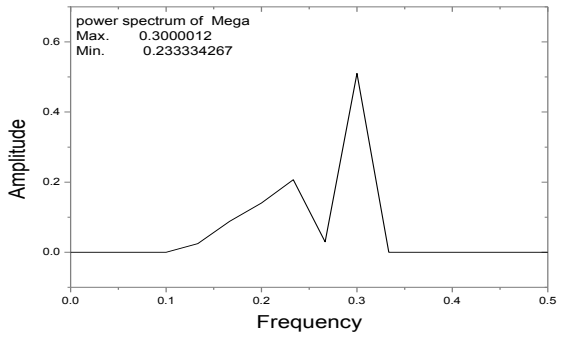
power spectrum of Mega
Max. 0.3000012
Min. 0.233334267
Amplitude
Frequency

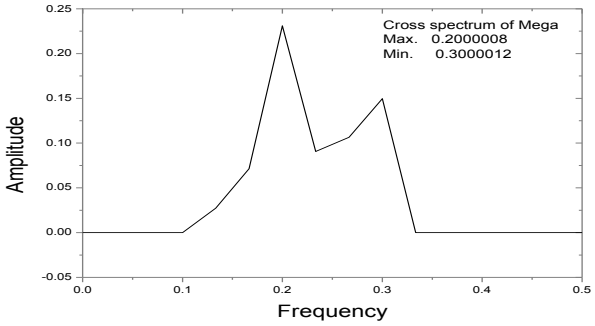
Cross spectrum of Mega
Max. 0.2000008
Min. 0.3000012
Amplitude
Frequency

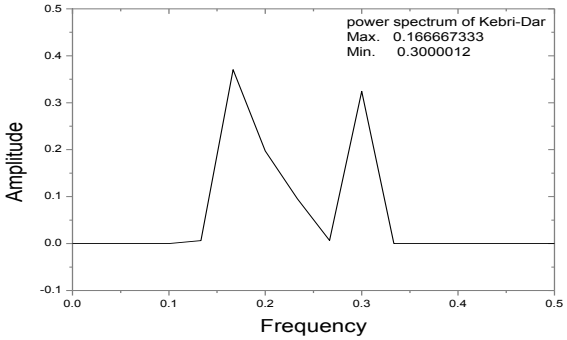
power spectrum of Kebri-Dar
Max. 0.166667333
Min. 0.3000012
Amplitude
Frequency

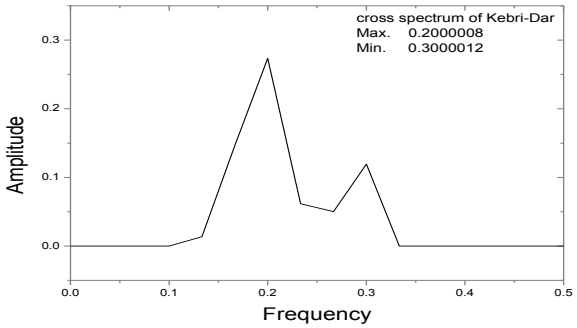
cross spectrum of Kebri-Dar
Max. 0.2000008
Min. 0.3000012
Amplitude
Frequency

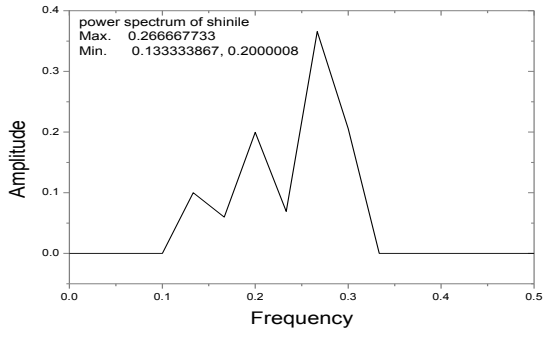
power spectrum of shinile
Max. 0.266667733
Min. 0.133333867, 0.2000008
Amplitude
Frequency

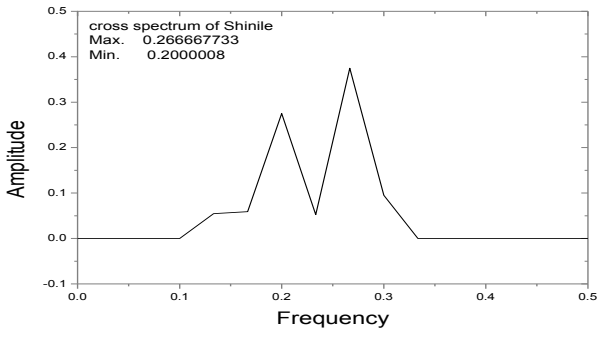
cross spectrum of Shinile
Max. 0.266667733
Min. 0.2000008
Amplitude
Frequency

Declaration

This thesis is my original work, has not been presented for a degree in any other University and that all the sources of material used for the thesis have been fully acknowledged.

Name: Robel Getachew Worku

Signature:_____

Place and time of submission: Addis Ababa University, June 2012

This thesis has been submitted for examination with my approval as University advisor.

Dr. Elias Lewi

Signature:_____